

A measurement of H_0 from DESI DR1 using energy densities

Alex Krolewski,^{1,2,*} Andrea Crespi,^{1,2,3} Will J. Percival,^{1,2,3} Marco Bonici,^{1,2} Hanyu Zhang,^{1,2} and J. Aguilar⁴, S. Ahlen⁵, D. Bianchi^{6,7}, D. Brooks⁸, R. Canning⁹, E. Chaussidon⁴, T. Claybaugh⁴, A. Cuceu⁴, S. Cole¹⁰, A. de la Macorra¹¹, J. Della Costa^{12,13}, P. Doel⁸, J. Edelstein^{14,15}, S. Ferraro^{4,15}, A. Font-Ribera¹⁶, J. Forero-Romero^{17,18}, E. Gaztañaga^{19,9,20}, S. Gontcho a Gontcho^{4,21}, G. Gutierrez²², J. Guy⁴, H. Herrera-Alcántar^{23,24}, K. Honscheid^{25,26,27}, D. Huterer^{28,29}, M. Ishak³⁰, D. Joyce¹³, R. Kehoe³¹, D. Kirkby³², T. Kisner⁴, A. Kremin⁴, O. Lahav⁸, C. Lamman²⁷, M. Landriau⁴, L. Le Guillou³³, M. Levi⁴, M. Manera^{34,16}, A. Meisner¹³, R. Miquel^{35,16}, J. Moustakas³⁶, A. Muñoz-Gutiérrez¹¹, S. Nadathur⁹, G. Niz^{37,38}, N. Palanque-Delabrouille^{24,4}, C. Poppett^{4,14,15}, F. Prada³⁹, I. Pérez-Ràfols⁴⁰, G. Rossi⁴¹, L. Samushia^{42,43,44}, E. Sanchez⁴⁵, D. Schlegel⁴, M. Schubnell^{28,29}, J. H. Silber⁴, D. Sprayberry¹³, G. Tarlé²⁹, B. A. Weaver¹³, and H. Zou⁴⁶

¹Waterloo Centre for Astrophysics, University of Waterloo, Waterloo, ON N2L 3G1, Canada

²Department of Physics and Astronomy, University of Waterloo, Waterloo, ON N2L 3G1, Canada

³Perimeter Institute for Theoretical Physics, 31 Caroline St. North, Waterloo, ON N2L 2Y5, Canada

The affiliations of the remaining authors are listed in Appendix D.

We present a new measurement of the Hubble constant, independent of standard rulers and robust to pre-recombination modifications such as Early Dark Energy (EDE), obtained by calibrating the total energy density of the Universe. We start using the present-day photon density as an anchor, and use the baryon-to-photon ratio from Big Bang Nucleosynthesis based measurements and the baryon-to-matter ratio from the baryons' imprint on galaxy clustering to translate to a physical matter density at present day. We then compare this to measurements of the ratio of the matter density to the critical density (Ω_m), calculated using the relative positions of the baryon acoustic oscillations, to measure the critical density of the universe and hence H_0 . The important measurements of the evolution of the energy density all happen at low redshift, so we consider this a low-redshift measurement. We validate our method both on a suite of N -body mocks and on noiseless theory vectors generated across a wide range of Hubble parameters in both Λ CDM and EDE cosmologies. Using DESI DR1 data combined with the angular CMB acoustic scale and the latest BBN constraints, we find $H_0 = 69.0 \pm 2.5 \text{ km s}^{-1} \text{ Mpc}^{-1}$, consistent with existing early and late-time determinations of the Hubble constant. We consider the impact of non-standard dark energy evolution on our measurement. Future data, including that from further iterations of DESI and from Euclid, will add to these results providing a powerful test of the Hubble tension.

I. INTRODUCTION

The Λ CDM model has been incredibly successful at explaining cosmic microwave background and large-scale structure measurements, with its parameters constrained to very high precision [1–3]. However, a potential crack has emerged with the high-significance tension between local measurements of the Hubble constant using the local distance ladder from Cepheids calibrating type Ia supernovae [4], $H_0 = 73.04 \pm 1.04 \text{ km s}^{-1} \text{ Mpc}^{-1}$, and cosmological inference in the Λ CDM model from Planck CMB measurements, $H_0 = 67.37 \pm 0.54 \text{ km s}^{-1} \text{ Mpc}^{-1}$. Large-scale structure measurements from the baryon acoustic oscillation (BAO) standard ruler favor a similarly low H_0 measurement (when calibrated by BBN), with $H_0 = 68.53 \pm 0.80 \text{ km s}^{-1} \text{ Mpc}^{-1}$ from DESI DR1 [5] and $68.51 \pm 0.58 \text{ km s}^{-1} \text{ Mpc}^{-1}$ from DESI DR2 [6]. This difference could be due to new physics [7] or systematics in one or more datasets [8].

A number of alternative H_0 measurements have been made with different distance ladder calibrators or other astrophysical objects entirely. Using the Tip of the Red

Giant Branch and J-Region Asymptotic Giant Branch stars in addition to Cepheids, [9] find $H_0 = 70.0 \pm 1.54 \text{ km s}^{-1} \text{ Mpc}^{-1}$ (adding their statistical and systematic errors in quadrature). On the other hand, [10] find a slightly higher value of H_0 from these same three calibrators in JWST data, $H_0 = 72.6 \pm 2.0 \text{ km s}^{-1} \text{ Mpc}^{-1}$. Other alternative methods are promising for the future but currently less constraining. For example, lensing time delays are statistically powerful but systematically limited by degeneracies with the mass profile [11]. Constraining H_0 from the single standard siren GW170817 achieves a $\sim 15\%$ precision [12], with considerable improvements possible by using outflow emission to constrain its inclination angle [13–15]. This method could be quite powerful in the future if a larger sample of GW events with confirmed counterparts can be discovered.

A popular class of new physics resolutions to the Hubble tension involves models that change the sound horizon r_d [16]. One such model involves adding a new component of “early dark energy” modifying the expansion rate around recombination [17, 18] (see also its relatives New Early Dark Energy [19] and Early Modified Gravity [20]). Other possibilities include modifications to the recombination history [21, 22], such as primordial magnetic fields [23], or variations in the electron mass [24] (see also [25] for a comprehensive comparison of various

* akrolews@uwaterloo.ca

theoretical solutions to the Hubble tension).

These models have motivated cosmological H_0 constraints from large-scale structure independent of the sound horizon, by marginalizing over an additional parameter scaling r_d [26–30]. Recent sound horizon-free measurements from CMB lensing cross-correlations [31] and the DESI DR1 power spectrum [32] have found H_0 consistent with other cosmological measurements, $64.3^{+2.1}_{-2.4}$ and $67.9^{+1.9}_{-2.1}$ km s^{−1} Mpc^{−1} respectively.¹ Combining these constraints, and replacing Ω_m information from supernovae with DESI DR1 BAO and the angular acoustic scale from the CMB, yields $H_0 = 69.2^{+1.3}_{-1.4}$ km s^{−1} Mpc^{−1} [33]. A similar method from [34], using uncalibrated BAO plus shape information from the model-agnostic ShapeFit method [35, 36], yields $H_0 = 70.1^{+1.9}_{-2.1}$ from the BOSS and eBOSS galaxy power spectrum. Finally, [37] measured the power spectrum turnover scale in the BOSS quasar power spectrum. Since they only use the turnover scale itself and not any shape information on smaller scales, their H_0 constraint is considerably weaker, $72.9^{+10.0}_{-8.6}$ km s^{−1} Mpc^{−1}.

These constraints generally assume a Λ CDM model for the shape of the power spectrum, beyond the marginalization over r_d . If a Hubble-tension-resolving modification also changes the shape of the power spectrum (e.g. as shown for EDE in [38]), it could shift these sound horizon-independent constraints. For instance, [39] find that the sound horizon marginalized constraints on H_0 , when analyzed in an early dark energy cosmology, shift towards higher values of H_0 by $\Delta H_0 = 3.8$ km s^{−1} Mpc^{−1} and the error nearly doubles. [40] also finds that sound horizon independent H_0 constraints can be consistent with a high value of the Hubble constant. Likewise, the constraints of [34] are also somewhat model dependent: allowing for a wide prior on n_s , freeing the neutrino mass, or adding ΔN_{eff} broadens their constraint to $\sigma_{H_0} = 2.5$ (3.2, 2.5) km s^{−1} Mpc^{−1}, while leaving the central value largely unchanged except for $\nu\Lambda$ CDM, which increases H_0 to 73.3 km s^{−1} Mpc^{−1}.

In light of these concerns, an alternative H_0 measurement has been proposed that limits the processes modeled to the very robust physics driven by the background energy densities of the Universe [41–43]. Specifically, the measurement is anchored to the extremely precise measurement of the CMB photon density; it then uses BBN based measurements to constrain the baryon-to-photon ratio and galaxy clustering to constrain the baryon fraction Ω_b/Ω_m ; together these give the physical matter density at present day. When comparing against Ω_m from the low redshift geometry of the Universe (e.g. BAO or supernovae), this allows us to infer the critical energy density of the Universe, which directly gives H_0 . In [41],

this method was explicitly shown to recover unbiased measurements of H_0 in EDE cosmologies with different true values of H_0 , showing that it is unbiased by any broadband shifts in the galaxy power spectrum due to the early-time new physics.

This method has previously been applied to the BOSS data, finding $H_0 = 67.1^{+6.3}_{-5.3}$ km s^{−1} Mpc^{−1}, limited by the precision of the baryon fraction [41, 42]. In this work, we improve the constraining power on the baryon fraction (and thus H_0) using data from DESI DR1. We also use a new, more robust pipeline to self-consistently model the baryon fraction, described in our companion paper [43].

In Section II, we describe the data used in this work and summarize the baryon fraction fitting pipeline. We test our pipeline on mocks in Section III A for our fiducial pipeline using Effective Field Theory fits to the power spectrum, and in Section III B using an alternative pipeline fitting to only the BAO in the post-reconstruction correlation function. We test on both the same N -body mocks used to validate the DESI full-shape measurements, and on a wide range of noiseless theory vectors in Λ CDM and EDE cosmologies. Finally, in Section IV, we describe our cosmological constraints from the DESI DR1 data. We did not run our pipeline on data until all of the mock tests in Section III A and III B were satisfied.

Throughout, all power spectra and correlation functions are measured using the DESI fiducial cosmology, with $\Omega_b h^2 = 0.02237$, $\Omega_c h^2 = 0.1200$, $h = 0.6736$, $A_s = 2.083 \times 10^{-9}$, $n_s = 0.9649$, and a single massive neutrino with mass 0.06 eV.

II. METHODS

A. Measuring H_0 from energy densities

Our method to measure H_0 is straightforward: we estimate the critical energy density of the Universe at present day, and therefore H_0 . The method can be summarized with this relation:

$$\frac{3c^2 H_0^2}{8\pi G} = \epsilon_c = \underbrace{\epsilon_{\gamma,0}}_{(i)} \times \underbrace{\frac{\epsilon_{b,0}}{\epsilon_{\gamma,0}}}_{(ii)} \times \underbrace{\frac{\epsilon_{m,0}}{\epsilon_{b,0}}}_{(iii)} \times \underbrace{\frac{1}{\Omega_{m,0}}}_{(iv)}, \quad (1)$$

where ϵ refers to a background energy density. Methods to robustly measure (i), (ii) and (iv) from simple physical measurements have already been developed using existing data; (i) can be measured from the CMB temperature, (ii) from BBN constraints on the photon-baryon ratio, and (iv) from geometric measurements of Ω_m . It was recently shown that (iii) can be measured in a robust way from galaxy clustering [41]. This measurement relies on the fact that the gravitational growth of perturbations is driven by the summed potential of baryons and dark matter. As a result, the amplitude of baryon effects in the low-redshift matter power spectrum depends only on the baryon fraction.

¹ We quote the constraints of [32] using Ω_m constrained by Pantheon+ supernovae; using Union3 supernovae gives a very similar H_0 measurement while using DESY5 supernovae shifts H_0 by 1.2 km s^{−1} Mpc^{−1}.

In order to extract the baryon fraction from only the effect of the growth of perturbations, we adopt a new procedure [43]. This procedure adds an additional parameter γ_b that changes the relative weighting of the baryon and CDM components in the gravitational potential adopted by the Boltzmann solver CAMB, which models the evolution of perturbations in time. Although unphysical, when γ_b is treated as a free parameter, this approach allows us to extract the baryon fraction from only the growth of perturbations in a fit to data. Performing a full fit with galaxy clustering data and extracting the constraint on the cosmological parameters Ω_b/Ω_m would bring in additional information on Ω_b (such as from the positions of the BAO peaks), complicating the interpretation as multiple physical processes contribute to the measurement.

We are able to constrain γ_b in a fit because the growth of baryonic perturbations is different from the growth of CDM perturbations, leading to features in the combined matter power spectrum, the amplitude of which depend on γ_b . In particular, the baryon perturbations can't grow before decoupling due to radiation pressure from the photons, but instead oscillate with the photons leading to a series of peaks and troughs in the power spectrum of the baryons perturbations as a function of scale, called Baryon Acoustic Oscillations (BAO). In addition to the oscillating signal, since baryon perturbations don't grow before decoupling, a larger baryon fraction suppresses the power spectrum on scales smaller than the sound horizon. On the other hand, the CDM perturbations begin to grow earlier, after matter-radiation equality.

To obtain this information, we previously [41] approximated these effects by splitting the linear power spectrum into baryon and CDM transfer functions. We then allowed γ_b to re-weight the sum of the transfer functions. However, this approach relies on ambiguous definitions of the baryon and CDM transfer functions. In this work, when constraining the baryon fraction from the full shape of the power spectrum (using the Effective Field Theory of large scale structure), we use the new approach of [43]. In this approach, the new parameter γ_b directly and self-consistently affects the growth of perturbations in the Boltzmann solver CAMB. This is described in detail in our companion paper [43].

B. Data used in our analyses

The Dark Energy Spectroscopic Instrument (DESI) [44, 45] is conducting an eight-year survey across 17,000 deg^2 [46], with the goal of updated goal of spectroscopically confirming 63M galaxies. To obtain these spectra, 5,000 fibers [47] are robotically positioned across a 7 deg^2 field [48, 49] using the Mayall 4-m telescope at Kitt Peak National Observatory [50]. Survey operations and assignment to DESI tiles are described in [46]. Once observed, spectra are processed with an automated spectroscopic reduction pipeline [51], and redshifts are determined automatically for all targets [52].

In this work, we use catalogs and clustering measurements from the first year of DESI observations, DESI DR1 [53, 54]. We use measurements of the pre-reconstruction power spectrum and the post-reconstruction correlation function. In both cases, we use the two-point functions calculated for analyses of the full-shape [55] and BAO position [5] signals. These papers contain more details about the analysis choices, which we summarize here. Clustering measurements were calculated using weights on each galaxy that mitigated the impact of imaging systematics, redshift failures, and incompleteness due to fiber collisions (see [54] for a comprehensive description of these weights), and optimise the signal. The power spectrum multipoles are fit in the k range $[0.02, 0.20] h \text{ Mpc}^{-1}$. Fiber collisions are mitigated by the ‘ θ -cut’ method, which removes all pairs separated by angular scales $< 0.05^\circ$ [56].

When we fit to the post-reconstruction correlation function, we jointly extract the baryon fraction and BAO positions required to constrain Ω_m . When we fit the power spectrum, we combine with pre-computed AP parameters from post-reconstruction BAO to determine Ω_m , using a joint covariance estimated from 1000 EZ-Mock [57] power spectrum and AP parameter measurements. An empirical scaling factor was applied to the covariance matrix, to account for inaccuracies in the EZ-Mocks and approximate fiber assignment [55]. A systematic error covariance accounts for imaging systematics, fiber assignment, and HOD-dependent systematics and prior-weight effects [58]. For our fiducial analysis in which we measure the BAO amplitude from the full-shape of the galaxy power spectrum, we use the LRG3 BAO measurement at $0.8 < z < 1.1$ rather than the ELG+LRG measurement used in [5] for ease of calculating the covariance between the post-reconstruction correlation function and the pre-reconstruction power spectrum. We also include the Ly α forest BAO measurement at $z = 2.33$ [59].

When fitting γ_b to the post-reconstruction correlatio function, we use a broader scale range than the DESI analysis [5] ($28 < r < 180 h^{-1} \text{ Mpc}$, since our pipeline includes an additional broadband term that is better constrained with the broader scale range. For these fits, we do not include a correction for fiber assignment, since the BAO scale is well-separated from the small scales impacted by fiber collisions. Covariances were computed analytically [60].

The analysis pipelines were validated using mock data from the Abacus-2 mocks (described in Section 3.1 of [61]) These were produced from the large suite of high-resolution N -body AbacusSummit simulations [62, 63]. Galaxies, with HODs chosen to match DESI, were populated into the 25 base boxes, generated with a Planck ΛCDM cosmology in a $(2 h^{-1} \text{ Gpc})^3$ box. These mocks were processed through the DESI survey geometry, and were generated with realistic runs of the fiber assignment process (“altmtl”) [64].

We use the θ_* measurement from Planck PR3, $100\theta_* =$

104.089 ± 0.031 (the “combined” constraint from [1]). We also include a constraint on the physical baryon density from Big Bang Nucleosynthesis (BBN) [65], $\Omega_b h^2 = 0.02218 \pm 0.00055$. We choose the BBN measurement of $\Omega_b h^2$ to be as independent of the CMB as possible. This measurement relies on primordial deuterium and helium measurements (as compiled by the Particle Data Group [66]) and nuclear rates from the `PRyMordial` code [67]. This measurement is quite insensitive to additional relativistic species ΔN_{eff} , and uncertainties in the reaction rates as well as systematic errors in the abundances are already marginalized over.

C. Energy density H_0 in EFT fits to the power spectrum

We constrain H_0 using Equation 1 by adding new “density” parameters h^{dens} , ω_b^{dens} and Ω_m^{dens} to our analysis. These are used in the analysis in such a way that they only depend on the physical processes selected. By treating the standard cosmological parameters H_0 , Ω_m , $\Omega_b h^2$, n_s and A_s as nuisance parameters to be marginalized over, we extract only the information required by Equation 1 using the desired physical processes, but can still perform a joint fit.

BBN information on ω_b^{dens} is implemented as a Gaussian prior. As a result, we will often refer to our analysis as including only two new parameters (h^{dens} and Ω_m^{dens}) and won’t show ω_b^{dens} contours in our tests on mocks.

From h^{dens} and ω_b^{dens} we define γ_b :

$$\gamma_b = \frac{\omega_b^{\text{dens}}}{\Omega_m^{\text{dens}}(h^{\text{dens}})^2 - \omega_{\text{massive-}\nu}} \quad (2)$$

where $\omega_{\text{massive-}\nu}$ is the density of massive neutrinos, for which we fix the neutrino mass at 0.06 eV. We then insert γ_b into our modified version of CAMB and use the resulting linear power spectrum as the input for the perturbative model of galaxy clustering.

The geometric information we include is the relative BAO positions, compressed to the Alcock-Paczynski parameters α_{iso} and α_{AP} and fitted to the post-reconstruction correlation function. We isolate the anisotropic information by marginalizing over the isotropic BAO position using an extra free parameter to model these measurements only. The model values of $H(z)$ and $D_A(z)$ required to fit these data are calculated using Ω_m^{dens} .

We use the Effective Field Theory of large scale structure (EFT of LSS) to model the galaxy power spectrum monopole and quadrupole. Specifically, we model the galaxy power spectrum using the Eulerian EFT formalism implemented in `VELOCILEPTORS` [68, 69] and emulated by `EFFORT.JL` [70]. The galaxy power spectrum model uses a symmetry-based bias expansion with linear and second-order bias parameters, counterterms and stochastic parameters to marginalize over unknown small-scale physics. We do not consider relative velocity

biases [e.g. 71–73] in our model. These biases can cause offsets in the BAO peak positions and thus potentially affect inference of the baryon fraction. Their effect is expected to be small compared to our current precision on the baryon fraction, but may need to be marginalized over in the future. An approximate estimate of their effect is given in Appendix A, and full implementation is left for future work.

The `VELOCILEPTORS` Eulerian EFT model uses 1-loop resummed Eulerian perturbation theory (REPT) where the linear and next-to-leading order terms are split into wiggle and no-wiggle components (following the method of [74]) and the wiggle part is exponentially damped with some dispersion Σ that is a function of the linear power spectrum. This is described in detail in Appendix A of [68]. While in principle the damping Σ may be degenerate with γ_b , we found this was not the case when fitting to the BOSS pre-reconstruction correlation function in [41]; we additionally found that BAO reconstruction reduces Σ but does not appreciably improve the constraining power on γ_b . We further test the sensitivity of our results to changing Σ and find this makes little difference—showing that our method is not very sensitive to the details of IR resummation.

We use the same model as the one used in the DESI DR1 full-shape analysis [55]. In our previous work [41], we used `CLASS-PT` instead, a different code also using Eulerian EFT to model the galaxy power spectrum. In Appendix B, we extensively compare to the old pipeline and show that it recovers the same results.

In a Bayesian analysis with a large number of poorly constrained nuisance parameters entering the likelihood nonlinearly, prior volume projection effects [75–77] are a generic issue. Projection effects are shifts in the marginalized likelihood relative to the posterior maximum (MAP). They can cause biases in marginalized posteriors when testing on mock datasets, even if the MAP is unbiased. They were extensively studied in the context of the DESI DR1 Λ CDM and $w_0 w_a$ CDM full-shape constraints in [55, 78]. In our analysis, adding two extra cosmological parameters (Ω_m^{dens} and h^{dens}) makes the projection effects even more severe.

We therefore impose Halo Occupation Distribution (HOD) informed priors [79–82] on the bias, counterterm, and stochastic parameters, allowing us to nearly eliminate projection effects (as shown in Sec. III A below). This method maps broad priors on HOD models of galaxy formation to EFT nuisance parameters, reducing the volume of unphysical nuisance parameters and thereby markedly reducing projection effects [79]. We follow the implementation of [79, 82], who trained a normalizing flow model to learn the mapping from broad HOD priors to priors on the EFT nuisance parameters. In [43], we show that the HOD prior recovers unbiased cosmology when fitting noiseless theory vectors where the growth and cosmological baryon fractions differ (even though the HOD prior was trained on standard cosmology where these two coincide).

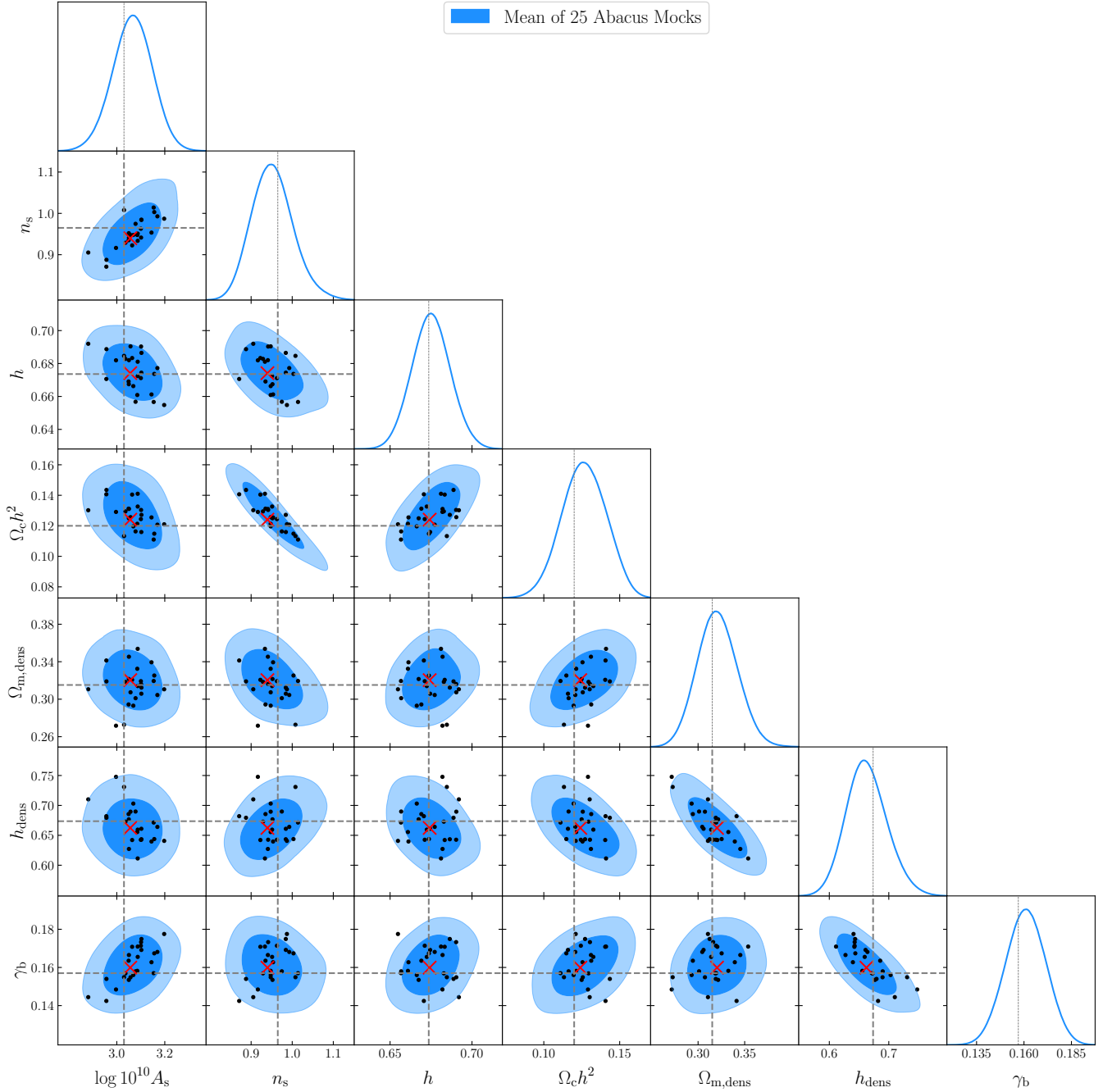


FIG. 1. Constraints on Λ CDM parameters and the Hubble parameter h^{dens} derived from the combination of energy densities, using the mean of the 25 Abacus mocks (truth in dashed lines). The red crosses show the maximum of the posterior. Black dots show marginalized means from the individual mocks.

Because we use EFFORT.JL, we can take advantage of other high-performance, state-of-the-art tools in JULIA to dramatically decrease the runtime of our analysis. The likelihood built from EFFORT.JL is automatically differentiable. We sample using the No U-Turn Sampler (NUTS) [83].

D. Energy density H_0 in post-reconstruction BAO fits

Although we adopt the full clustering fits as our baseline, we compare against results fitting just the post-reconstruction BAO signal as a test of the robustness of our method. For these we use the method of [43] to create linear power spectra including the γ_b parameter to

control the baryon fraction in gravitational perturbation growth.

We use this linear matter power spectrum as input to the method of [73] to extract BAO positions from the post-reconstruction correlation function. This splits the linear power spectrum into wiggle ($P_w(k)$) and no-wiggle ($P_{nw}(k)$) parts. The post-reconstruction correlation function is then modelled with a damped linear power spectrum

$$P(k, \mu) = \mathcal{B}(k, \mu)P_{nw}(k) + \mathcal{C}(k, \mu)P_w(k) + \mathcal{D}(k, \mu) \quad (3)$$

where $\mathcal{B}(k, \mu)$ matches [5] with an additional term proportional to $b_\partial k^2$ [84]:

$$\mathcal{B}(k, \mu) = \left((b_1 + f\mu^2)^2 + b_\partial \frac{k^2}{k_L^2} (b + f\mu^2) \right) \times \left(\frac{1}{1 + 0.5k^2\mu^2\Sigma_s^2} \right)^2 \quad (4)$$

and $\mathcal{C}(k, \mu)$ is exactly the same as in [5]

$$\mathcal{C}(k, \mu) = (b_1 + f\mu^2)^2 \exp \left[-\frac{1}{2}k^2 \left(\mu^2\Sigma_\parallel^2 + (1 - \mu^2)\Sigma_\perp^2 \right) \right] \quad (5)$$

The broadband term $\mathcal{D}(k, \mu)$ is identical to the spline basis used in [5]:

$$\mathcal{D}_\ell(k) = \sum_{n=-1}^{n_{\max}} a_{\ell,n} W_3 \left(\frac{k}{\Delta - n} \right) \quad (6)$$

where W_3 is a piecewise cubic spline kernel, $\Delta = 2\pi/r_d = 0.06 h \text{ Mpc}^{-1}$, and $n_{\max} = 7$. This is an update on the method used in [41], which adopted polynomial broadband terms, which we found to be quite degenerate with the BAO amplitude, particularly the $1/s^2$ term. In contrast, the cubic spline basis is not degenerate with the BAO amplitude by construction, as it marginalizes over any (Fourier-space) oscillatory component with a higher frequency than the BAO as well as large scale systematics from Fourier modes with $k < k_{\min}$. Therefore, we use the same cubic spline broadband parameters as [5], with two terms affecting the monopole (a constant and s^2 term) and four terms affecting the quadrupole (constant, s^2 , and Hankel transforms of the two lowest-order spline terms). We apply the same priors as [5], a flat infinite prior on the constant and s^2 terms and $\mathcal{N}(0, 10^4)$ on the spline parameters.

We also match the treatment of [73] and apply the Finger-of-God small-scale RSD term to the no-wiggle power spectrum only, rather than to both the wiggle and no-wiggle power spectrum as in BOSS and our previous analysis [41]. We also replace the narrow Gaussian prior on b_∂ from [41] (15 ± 5) with a broad flat prior between -1000 and 1000 , increasing the fitted range to $28 < r < 180 h^{-1} \text{ Mpc}$ to provide the necessary extra constraining power on b_∂ . Finally, we use the ‘‘RecSym’’ reconstruction convention [85, 86] with $\Sigma_{\text{sm}} = 15 h^{-1}$

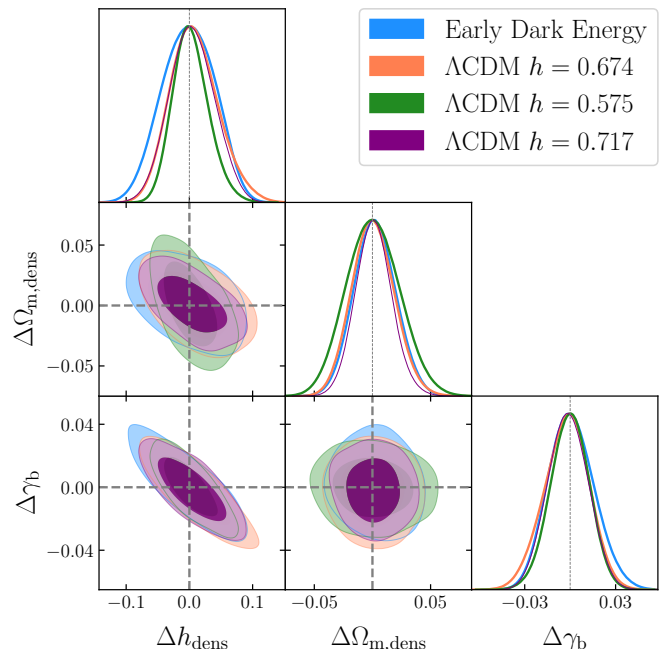


FIG. 2. Our method accurately recovers the Hubble parameter across a wide range in true h , and in both a Λ CDM and an Early Dark Energy cosmology (with $h = 0.722$).

Mpc for all tracers except QSO, for which $\Sigma_{\text{sm}} = 30 h^{-1} \text{ Mpc}$ is used [87], rather than ‘‘RecIso’’ [88] for all tracers, allowing a much simpler model for the post-reconstruction correlation function with only a single Gaussian damping terms with line-of-sight and transverse damping scales. Rather than tying together the damping terms with Σ_{sm} as in [41], we now allow Σ_\perp and Σ_\parallel to vary separately with broad flat priors.

III. MOCK TESTS

A. Testing the EFT model fit

We refer the reader to our companion paper [43], for a battery of extensive tests of the new method, investigating the recovered parameters for many mock power spectra. We highlight a few of the tests here by showing, in Fig. 1, that we can accurately recover γ_b (and thus the density-derived Hubble parameter h^{dens}) when fitting to the mean of the 25 Abacus mocks. As detailed in Table I, we find biases of $< 0.3\sigma$ in both h^{dens} and γ_b , and good agreement between the marginalized mean and the maximum of the posterior. We also find that the spread among the 25 Abacus mocks is consistent with the reported errors.

We have also verified our recovery of the baryon fraction on noiseless theory vectors spanning a wide range in input Λ CDM and Early Dark Energy cosmologies. As shown in Fig. 2, our method recovers the correct baryon

Mock	Truth		h		γ_b	
	h	f_b	Mean $\pm 1\sigma$ (MAP)	$n\sigma$	Mean $\pm 1\sigma$ (MAP)	$n\sigma$
Abacus	0.6736	0.1571	0.663 ± 0.033 (0.662)	-0.30	0.160 ± 0.011 (0.160)	0.26
Λ CDM Noiseless	0.6736	0.1571	0.681 ± 0.037 (0.677)	0.20	0.155 ± 0.0144 (0.155)	-0.14
EDE Noiseless	0.7219	0.1471	0.721 ± 0.040 (0.716)	-0.03	0.1479 ± 0.015 (0.150)	0.05

TABLE I. Summary of full-shape fits to the mean of the 25 Abacus mocks and noiseless theory vectors in both the default Λ CDM and early dark energy cosmologies.

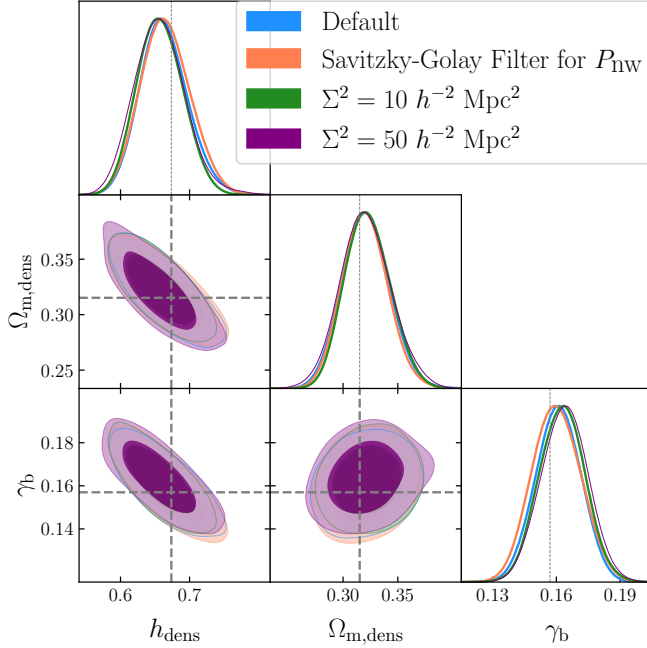


FIG. 3. The recovery of γ_b and h^{dens} on the pre-reconstruction power spectrum is not sensitive to the details of IR resummation. Here we compare the default result (on the mean of the 25 Abacus mocks) to runs where we change the filter used to construct the no-wiggle power spectrum (orange) or those where we change the damping of the wiggle power spectrum (green and purple).

fraction in a Λ CDM cosmology generated in the DESI fiducial cosmology, an Early Dark Energy cosmology with $h = 0.722$, and Λ CDM cosmologies with both high and low values of h . We show more extensive tests in [43], where we show that h and γ_b are biased by $< 0.1\sigma$ in both Λ CDM and EDE cosmologies across a broad range in true h , $0.55 < h < 0.8$.

In Fig. 3, we test the sensitivity of our results on the mean of the Abacus mocks to changing the IR resummation parameters. We test both changing the method for the IR resummation split (from the default method from [74] to using a Savitzky-Golay filter), and fixing the damping parameter to either $\Sigma^2 = 10 h^{-2} \text{ Mpc}^2$ or $\Sigma^2 = 50 h^{-2} \text{ Mpc}^2$ —roughly bracketing the default value of $\Sigma^2 \sim 30$ for all tracers in the default DESI cosmology. We find that these changes minimally affect our results, changing H_0 by $< 0.25\sigma$, and conclude that our method

is robust to the IR resummation method used.

B. Testing the post-reconstruction BAO fits

Given the changes in our pipeline fitting γ_b to the post-reconstruction correlation function, we have also undertaken a series of tests of the revised method. We find that our pipeline accurately recovers the true value of γ_b (Fig. 4) and matches the DESI DR1 fits to the Abacus mocks well (Fig. 5). We compare the BAO parameters to the DESI DR1 BAO fits in more detail in Appendix C, showing that the constraining power of our pipeline on α_{iso} is similar, but the α_{AP} constraints are slightly worse due to the larger number of free parameters in our model. We summarize the fits to each tracer in Table II, and show that the model fits the data well with χ^2 matching the expected number of degrees of freedom. The small residual differences between our results and the DESI DR1 pipeline can be attributed to slightly different nuisance parameter priors. In particular, our pipeline has slightly larger errors on α_{AP} due to the broad priors on the damping parameters Σ_{\parallel} , Σ_{\perp} , and Σ_{fog} .

Combining the fits to the mean of the 25 Abacus mocks, we find $\gamma = 0.159 \pm 0.0154$, a 0.11σ bias away from the truth in units of the DR1 errorbar. Since we have 25 Abacus mocks, the error on the mean is 5 times smaller, meaning that the bias is statistically consistent with zero.

We fit cosmological parameters to the compressed results from Table II, using the DESI DR1 measurements and covariance for α_{iso} and α_{AP} . We measure the cross-covariance between γ_b , α_{iso} and α_{AP} from the parameter covariance in our fits to the post-reconstruction correlation function. We find $h^{\text{dens}} = 0.679^{+0.044}_{-0.037}$ and $\gamma_b = 0.158 \pm 0.014$, in good agreement with the full-shape results although with less constraining power, as expected since we are not using any shape information. This is consistent with our previous results on BOSS, which showed that reconstruction changes the BAO damping parameter but does not tighten constraints on γ_b [41].

In Fig. 6, we compare the pre-reconstruction and post-reconstruction fits for γ_b on the 25 Abacus mocks. As expected, they are highly correlated, with a correlation coefficient of 0.6. We tested including the post-reconstruction γ_b in our data vector along with the post-reconstruction BAO parameters, using the 1000 EZ-mocks to measure the cross-covariance with the pre-reconstruction power spectrum. We find that this leads

Parameter	Truth	Fit to mean	Med. of 25 fits
BGS, $0.1 < z < 0.4$			
α_{iso}	1.0067	1.0057 ± 0.0226	1.0021 ± 0.0265
γ_b	0.1571	0.1362 ± 0.0449	0.1379 ± 0.0505
χ^2	29	1.0	28.3
LRG, $0.4 < z < 0.6$			
α_{iso}	1.006	1.0068 ± 0.0139	1.0121 ± 0.0154
α_{AP}	0.998	0.9990 ± 0.0534	1.0064 ± 0.0547
γ_b	0.1571	0.1633 ± 0.0358	0.1682 ± 0.0360
χ^2	59	3.7	53.4
LRG, $0.6 < z < 0.8$			
α_{iso}	1.0050	1.0056 ± 0.0112	1.0045 ± 0.011
α_{AP}	0.9978	1.0082 ± 0.0432	1.0084 ± 0.0392
γ_b	0.1571	0.1574 ± 0.0354	0.1554 ± 0.0331
χ^2	59	3.3	64.3
LRG+ELG, $0.8 < z < 1.1$			
α_{iso}	1.0044	1.0068 ± 0.0088	1.0082 ± 0.0085
α_{AP}	0.9974	1.0028 ± 0.0293	0.9934 ± 0.0277
γ_b	0.1571	0.1638 ± 0.0262	0.1559 ± 0.0262
χ^2	59	4.3	60.2
ELG, $1.1 < z < 1.6$			
α_{iso}	1.0036	1.0049 ± 0.0155	1.0068 ± 0.0160
α_{AP}	0.9971	0.9934 ± 0.0572	1.0008 ± 0.0555
γ_b	0.1571	0.1608 ± 0.0389	0.1610 ± 0.0372
χ^2	59	5.8	57.9
QSO, $0.8 < z < 2.1$			
α_{iso}	1.0033	1.0065 ± 0.0178	0.9961 ± 0.0179
γ_b	0.1571	0.1585 ± 0.0359	0.1529 ± 0.0377
χ^2	29	1.8	34.4

TABLE II. Recovery of BAO scaling parameters and γ_b on the post-reconstruction correlation function of 25 Abacus altmtl cutsky mocks, analyzed in the BOSS fiducial cosmology, and using the DESI data covariance. The first column gives the true value of each parameter, or the number of degrees of freedom for the dataset. The second column gives the result of a fit to the mean of the 25 mocks, using the DESI data covariance matrix. The final column gives the median and median of the errorbar of fits to each of the 25 different mocks. The fits to the mean have smaller χ^2 because we use the DESI DR1 covariance matrix everywhere. Combining the fits to the mean from each tracer gives $\gamma_b = 0.159 \pm 0.014$.

to only a 6% improvement in the constraining power on H_0 , consistent with the strong correlation between pre and post-reconstruction γ_b . Due to the minimal gain in constraining power and to avoid additional complexity regarding the impact of reconstruction on γ_b , we do not choose to combine the pre- and post-reconstruction γ_b by default.

IV. RESULTS AND DISCUSSION

After passing the validation tests described in [43] and in Sections III A and III B, we unblinded and performed the same fits on the data. Our fiducial full-shape based results are shown in Fig. 7 and summarized in Table III.

Using the DESI DR1 galaxy clustering data for the baryon fraction and Ω_m , and the latest BBN constraint on $\Omega_b h^2 = 0.02218 \pm 0.00055$ from [65], we find $H_0 = 68.4 \pm 3.6 \text{ km s}^{-1} \text{ Mpc}^{-1}$.

We find consistency between our fiducial method, inferring the baryon fraction from the full-shape of the power spectrum, and the alternative where we measure the baryon fraction from the post-reconstruction correla-

tion function. Specifically, the difference in H_0 between the two methods ($2.3 \text{ km s}^{-1} \text{ Mpc}^{-1}$) is consistent with the scatter expected due to the excess variance in the post-reconstruction method compared to the full-shape method ($2.7 \text{ km s}^{-1} \text{ Mpc}^{-1}$).² The full-shape method gives tighter errors on γ_b (and thus H_0), as expected because it incorporates baryon-fraction information from the shape of the power spectrum that is marginalized over by the broadband parameters in the post-reconstruction fits. $\Omega_{m,\text{dens}}$ is slightly different between the two methods because in the full-shape fits, we use the power spectrum and post-reconstruction AP parameters from the LRG3 bin at $0.8 < z < 1.1$, whereas in the post-reconstruction fits, we use the combined LRG+ELG correlation function at $0.8 < z < 1.1$.

When including DESI DR1 Ly α BAO, we find for our baseline DESI-only constraints, $H_0 = 68.6 \pm 3.1 \text{ km s}^{-1} \text{ Mpc}^{-1}$. We can further improve the constraints by also

² Determined as $\sqrt{4.5^2 - 3.6^2}$, the quadrature difference of the H_0 errors from the post-reconstruction γ_b and the full-shape γ_b

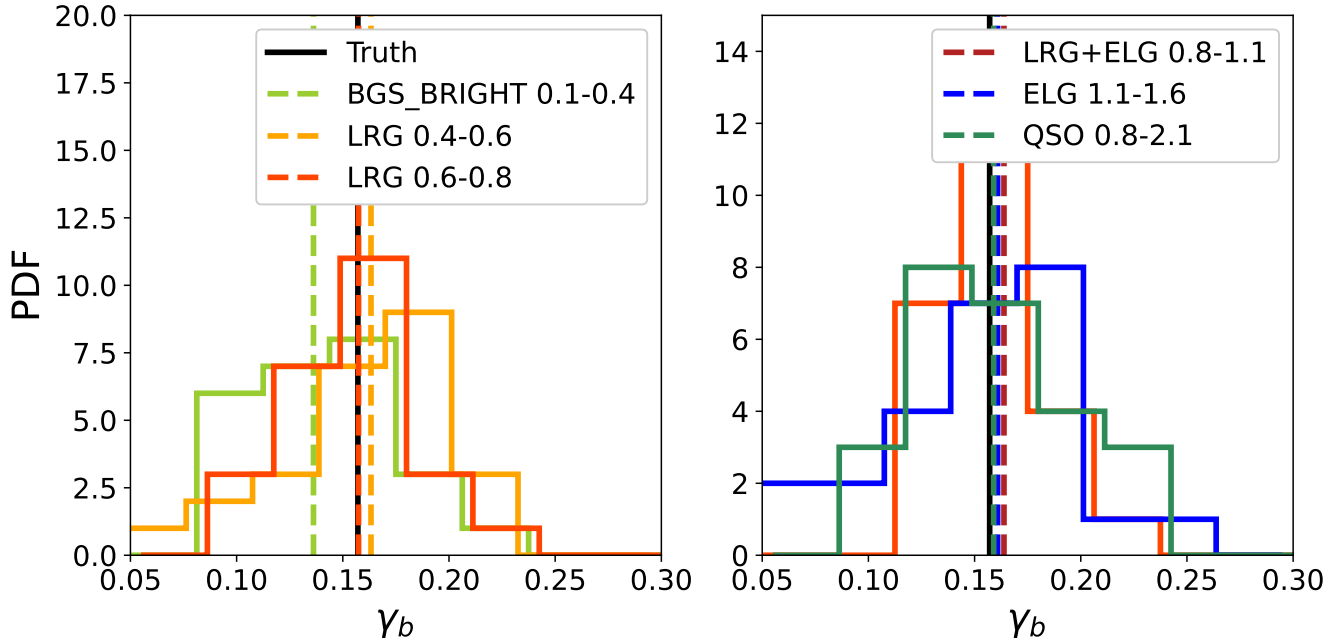


FIG. 4. Distribution of γ_b fit to the post-reconstruction correlation function of all DESI tracers in the 25 Abacus mocks; the tracers are split between the two panels for clarity. The solid black line shows the true value of the baryon fraction and the dashed lines show the fits to the mean of the 25 Abacus mocks.

Data combination	H_0^{dens} (km s $^{-1}$ Mpc $^{-1}$)	$\Omega_{\text{m,dens}}$	γ_b
DESI DR1 Galaxy clustering (Full Shape γ_b)	68.4 ± 3.6	0.301 ± 0.020	0.161 ± 0.010
DESI DR1 Galaxy clustering (Post-recon γ_b)	70.7 ± 4.5	0.294 ± 0.022	0.153 ± 0.014
DESI DR1 Galaxy clustering + Ly α	68.6 ± 3.1	0.301 ± 0.014	0.161 ± 0.010
DESI DR1 Galaxy clustering + Ly α + θ_*	69.0 ± 2.5	0.294 ± 0.007	0.161 ± 0.010

TABLE III. Constraints on density-derived cosmological parameters from DESI DR1. Top row shows our fiducial results, measuring γ_b from EFT modelling of the power spectrum, using DESI DR1 galaxy clustering data only. The middle row shows the results when we only use BAO amplitude information, measuring γ_b in the post-reconstruction correlation function and marginalizing over all shape information. The bottom row shows the fiducial method combined with DESI DR1 Ly α and Planck θ_* .

including Planck PR3 θ_* , effectively an additional angular BAO measurement at $z \sim 1090$. While there is some disagreement between Planck PR3 and DESI DR1 in the $\Omega_{\text{m}}-H_0 r_d$ plane, the tension is $< 2\sigma$, and it is worse in the $H_0 r_d$ direction (1.8σ) than Ω_{m} (1.2σ). It is therefore justified to combine these datasets.

When combining with θ_* , we find $H_0 = 69.0 \pm 2.5$ km s $^{-1}$ Mpc $^{-1}$. This is in good agreement (0.7σ tension) with the CMB constraints on H_0 in Λ CDM (67.24 ± 0.35 km s $^{-1}$ Mpc $^{-1}$ from [89]). Our measurement is also consistent with the local H_0 measurement from SH0ES (73.04 ± 1.04 km s $^{-1}$ Mpc $^{-1}$) [4], with a slightly larger difference of 1.5σ .

In our previous work, we used Type Ia supernovae as uncalibrated standard candles to further improve the geometric constraints on Ω_{m} . However, the Ω_{m} constraints from the supernovae are in modest tension with those from DESI and θ_* (1.9σ for Pantheon+, 2.2σ for Union3, and 3.5σ for DESY5SN). This tension is also manifested

in the $2-3\sigma$ preference for $w_0 w_a$ CDM over Λ CDM when combining DESI DR1, CMB, and supernovae. Given that we infer Ω_{m} from geometric probes assuming Λ CDM, we therefore opt not to combine with supernovae.

Combining with supernovae and infer Ω_{m} in an evolving dark energy cosmology, yields a larger Ω_{m} (0.323 ± 0.0095 using Union3 supernovae, from Table 3 in [5]). Scaling our results by $H_0 \propto \Omega_{\text{m}}^{-0.5}$ (from Eq. 1) leads to a smaller H_0 (66.0 km s $^{-1}$ Mpc $^{-1}$), but still in $\sim 2\sigma$ agreement with SH0ES. Ω_{m} is lower when combining with other supernovae samples, and this leads to smaller shifts in H_0 , to 66.7 km s $^{-1}$ Mpc $^{-1}$ with DESY5 or 67.5 km s $^{-1}$ Mpc $^{-1}$ with Pantheon+. While moving to a w_0-w_a cosmology reduces constraining power on Ω_{m} , the extra information from the supernovae compensates for this reduction and thus the Ω_{m} error is similar to when we include θ_* .

A nonzero spatial curvature could also mitigate the discrepancy between DESI and the CMB [90]. When

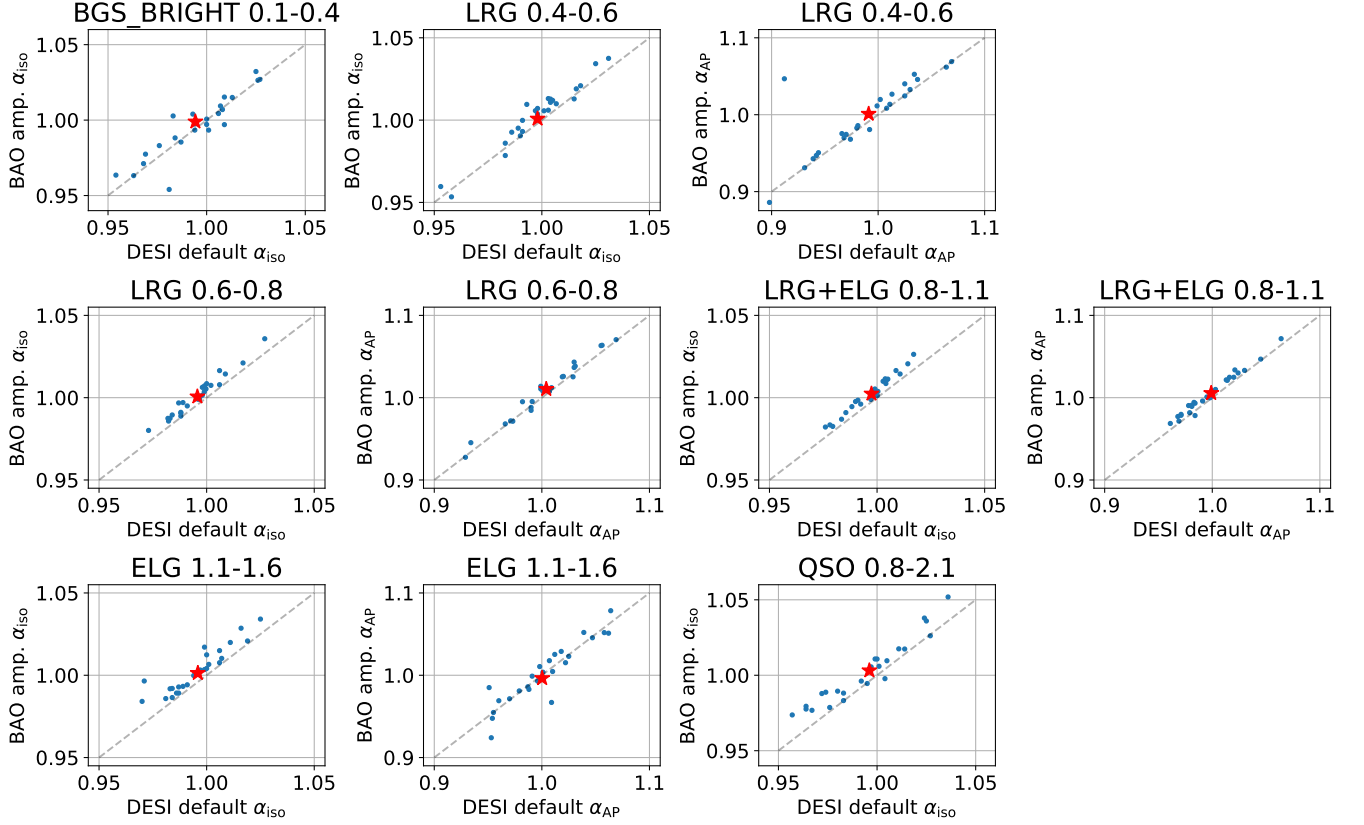


FIG. 5. Comparison between Alcock-Paczynski parameters, α_{iso} and α_{AP} , from the default DESI fits to the post-reconstruction correlation function, and fit using our pipeline with γ_b as a free parameter. Blue dots show the fit to each of the 25 Abacus mocks, while the red star shows the fit to the mean. The BAO amplitude fits have been rescaled to match the DESI fiducial cosmology. The dashed line indicates perfect agreement between the two pipelines.

Tracer	γ_b	α_{iso}	α_{AP}
BGS_BRIGHT 0.1-0.4	0.106 ± 0.050	0.981 ± 0.026	
LRG 0.4-0.6	$0.146^{+0.034}_{-0.037}$	0.986 ± 0.013	0.923 ± 0.040
LRG 0.6-0.8	$0.219^{+0.030}_{-0.036}$	0.967 ± 0.010	1.036 ± 0.039
LRG+ELG 0.8-1.1	0.157 ± 0.030	1.005 ± 0.008	1.027 ± 0.028
ELG 1.1-1.6	$0.156^{+0.041}_{-0.036}$	0.998 ± 0.014	0.971 ± 0.043
QSO 0.8-2.1	0.122 ± 0.037	1.017 ± 0.0250	

TABLE IV. Results on data from post-recon fits to each tracer. α_{iso} and α_{AP} are quoted relative to the DESI fiducial cosmology.

Ω_k is free, the Ω_m constraints from DESI + BBN + θ_* become considerably weaker (0.296 ± 0.014) but tighten when adding the full CMB likelihood (0.305 ± 0.0051) [5]. The small shift in Ω_m in a free curvature model would shift H_0 down to $\sim 68 \text{ km s}^{-1} \text{ Mpc}^{-1}$.

Freeing the neutrino mass does not change the inference of Ω_m much. The DESI + CMB Ω_m measurement changes from 0.3069 ± 0.0050 in ΛCDM to 0.3037 ± 0.0053 in $\nu\Lambda\text{CDM}$. Likewise, in $w_0w_a\text{CDM}$ (using Union3 supernovae, but results are similar for DES Y5 and Pantheon+), Ω_m changes from 0.323 ± 0.0095 to 0.324 ± 0.0098 when freeing the neutrino mass [5].

V. CONCLUSIONS AND OUTLOOK

We have applied a new method to infer the Hubble constant from the total energy density of the Universe, independent of standard rulers to DESI DR1 data. This method relies on comparing the physical matter density ϵ_m (from the CMB temperature, BBN, and the baryon fraction from galaxy clustering) with the fractional matter density Ω_m (from relative sizes of geometric probes). We show that this method is robust when applied both to the DESI DR1 Abacus mocks, and to noiseless theory vectors drawn from ΛCDM and Early Dark Energy cosmologies across a wide range in H_0 . This explicitly

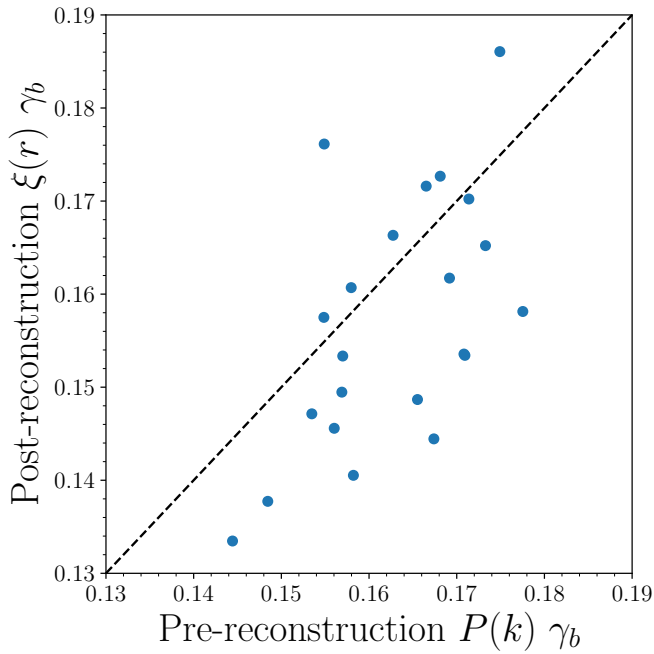


FIG. 6. Comparison between γ_b measurement from the pre-reconstruction power spectrum and the post-reconstruction correlation function for the 25 Abacus mocks.

shows that this method can be used to test models like EDE that resolve the Hubble tension by modifying the sound horizon.

We validate measurements of the baryon fraction both using the full-shape of the power spectrum fit with the EFT of Large Scale Structure (our fiducial method) and fitting the amplitude of the BAO feature in the post-reconstruction correlation function. For both methods, we have developed a new, more consistent method to consistently extract baryon fraction information from the dependence of the power spectrum on the gravitational component of the growth of structure (as described in our companion paper [43]). Both methods return consistent H_0 constraints both on mocks and on data, with our fiducial method returning tighter constraints as it includes full-shape information that is marginalized in the post-reconstruction BAO fitting.

When inferring Ω_m from the relative BAO positions in DESI and the CMB (i.e. θ_*), we find $H_0 = 69.0 \pm 2.5 \text{ km s}^{-1} \text{ Mpc}^{-1}$. This is consistent with both the Planck and SH0ES H_0 measurements, though closer to the Planck value.

The constraining power of our measurement is similar to other r_d -marginalized measurements from DESI DR1. Using the DESI DR1 power spectrum and CMB lensing, [32] find $H_0 = 70.1^{+2.7}_{-3.3} \text{ km s}^{-1} \text{ Mpc}^{-1}$, and $H_0 = 66.7^{+1.7}_{-1.9} \text{ km s}^{-1} \text{ Mpc}^{-1}$ when also using Ω_m information from DES-Y5 supernovae. Using the same methodology but replacing supernovae with DESI DR1 BAO and Planck θ_* , [33] finds $H_0 = 69.2^{+1.4}_{-1.3} \text{ km s}^{-1} \text{ Mpc}^{-1}$. Simi-

larly, using DESI DR2, CMB lensing, galaxy lensing, and supernovae, [91] finds $H_0 = 70 \pm 1.7 \text{ km s}^{-1} \text{ Mpc}^{-1}$. However, our method is more explicitly independent of pre-recombination H_0 modifications than these other works. The sound-horizon-marginalized method of [32, 33] infers H_0 by comparing Ω_m to $\Omega_m h^2$ inferred from the shape of the power spectrum (i.e. setting the power spectrum turnover scale, though they do not explicitly measure the turnover as they use $k_{\min} = 0.02 \text{ h Mpc}^{-1}$). However, new physics that alters the sound horizon can also change the broadband shape of the power spectrum, affecting inference of $\Omega_m h^2$ and thus H_0 [39]. Likewise, early dark energy can change the value of $\Omega_m h^2$ inferred from the CMB and would thus change H_0 inferred in [91]. In contrast, we show explicitly that our method recovers the correct value of H_0 in early dark energy cosmologies.

Our method is currently limited by the accuracy of the baryon fraction measurement; however, this is expected to improve greatly with current and future DESI data. The final DESI data will increase the sky coverage by 3-4 \times , as well as increasing completeness and number density (particularly critical for the dense ELG sample). These significant improvements will enable this measurement to differentiate between the local and cosmological H_0 measurements.

DATA AVAILABILITY

The data used in this work are public as part of DESI Data Release 1 (details at <https://data.desi.lbl.gov/doc/releases/>). The data points corresponding to the figures are available on Zenodo at <https://zenodo.org/uploads/17686137>. Code is available on github <https://github.com/drew2799/fbCMB>.

ACKNOWLEDGMENTS

AK was supported as a CITA National Fellow by the Natural Sciences and Engineering Research Council of Canada (NSERC), funding reference #DIS-2022-568580. WP acknowledges support from the Natural Sciences and Engineering Research Council of Canada (NSERC), [funding reference number RGPIN-2025-03931] and from the Canadian Space Agency. Research at Perimeter Institute is supported in part by the Government of Canada through the Department of Innovation, Science and Economic Development Canada and by the Province of Ontario through the Ministry of Colleges and Universities. This research was enabled in part by support provided by Compute Ontario (computeontario.ca) and the Digital Research Alliance of Canada (alliancecan.ca).

This material is based upon work supported by the U.S. Department of Energy (DOE), Office of Science, Office of High-Energy Physics, under Contract No. DE-AC02-05CH11231, and by the National Energy Research Scientific Computing Center, a DOE Office of

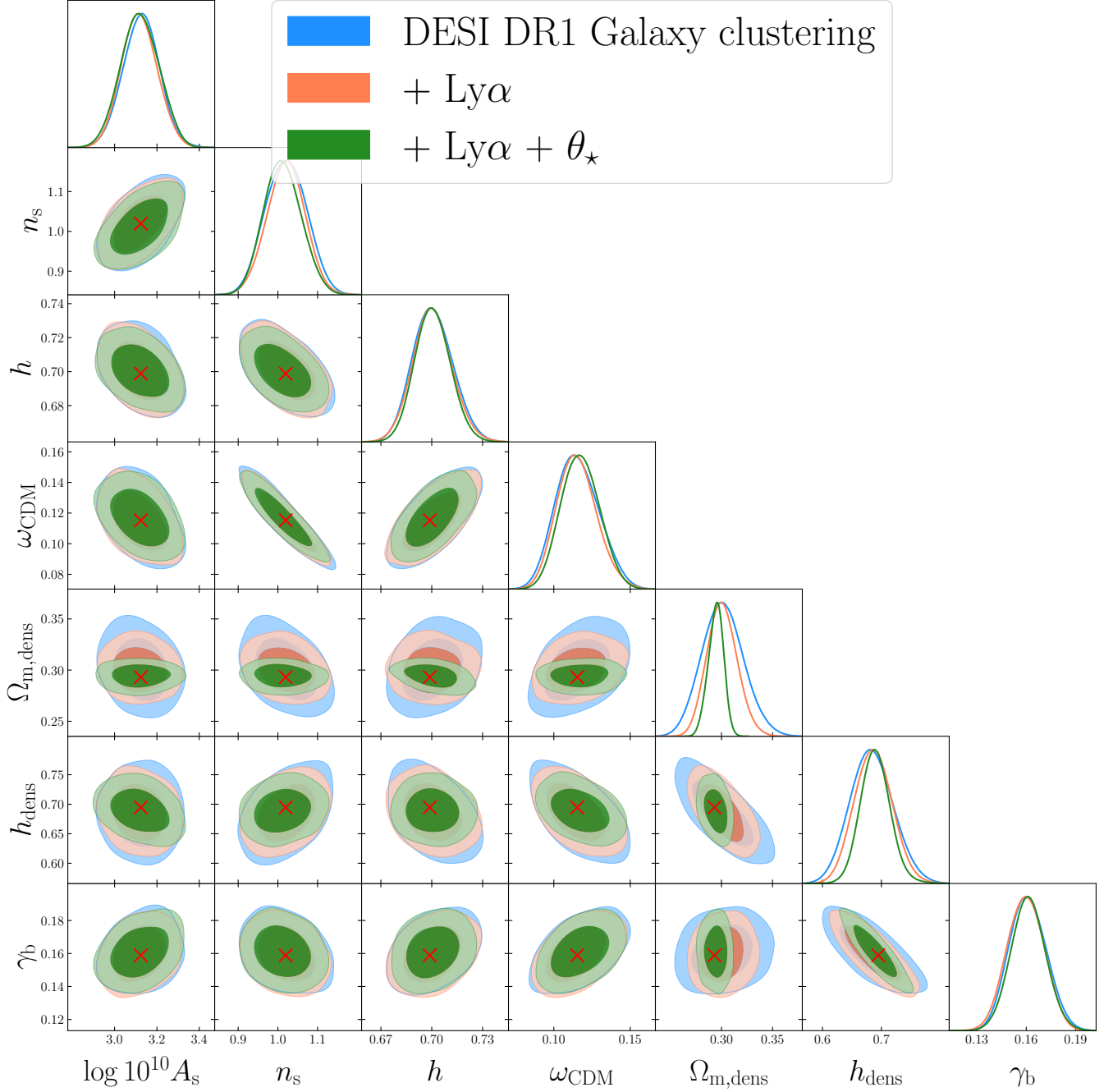


FIG. 7. Constraints on density-derived H_0 using DESI DR1 galaxy clustering data (blue), also including DESI DR1 Ly α (orange), and finally when also including Planck θ_* to improve the constraints on $\Omega_{\text{m,dens}}$ (green). The MAP point (when including Ly α and θ_*) is shown with red crosses.

Science User Facility under the same contract. Additional support for DESI was provided by the U.S. National Science Foundation (NSF), Division of Astronomical Sciences under Contract No. AST-0950945 to the NSF's National Optical-Infrared Astronomy Research Laboratory; the Science and Technology Facilities Council of the United Kingdom; the Gordon and Betty Moore Foundation; the Heising-Simons Founda-

tion; the French Alternative Energies and Atomic Energy Commission (CEA); the National Council of Humanities, Science and Technology of Mexico (CONACYT); the Ministry of Science, Innovation and Universities of Spain (MCIU/AEI/10.13039/501100011033), and by the DESI Member Institutions: <https://www.desi.lbl.gov/collaborating-institutions>. Any opinions, findings, and conclusions or recommendations expressed

in this material are those of the author(s) and do not necessarily reflect the views of the U. S. National Science Foundation, the U. S. Department of Energy, or any of the listed funding agencies.

The authors are honored to be permitted to conduct

scientific research on I'oligam Du'ag (Kitt Peak), a mountain with particular significance to the Tohono O'odham Nation.

Software: `getdist` [92], `desilike`³, `velocileptors` [68, 69], `Julia`, `Lux.jl` [93], `Turing.jl` [94, 95], `Effort.jl` [70], `CLASS-PT` [96], `baofit`⁴.

-
- [1] Planck Collaboration, N. Aghanim, Y. Akrami, M. Ashdown, J. Aumont, C. Baccigalupi et al., *Planck 2018 results. VI. Cosmological parameters*, *A&A* **641** (2020) A6 [1807.06209].
 - [2] DESI Collaboration, A.G. Adame, J. Aguilar, S. Ahlen, S. Alam, D.M. Alexander et al., *DESI 2024 VI: cosmological constraints from the measurements of baryon acoustic oscillations*, *J. Cosmology Astropart. Phys.* **2025** (2025) 021 [2404.03002].
 - [3] DESI Collaboration, A.G. Adame, J. Aguilar, S. Ahlen, S. Alam, D.M. Alexander et al., *DESI 2024 VII: cosmological constraints from the full-shape modeling of clustering measurements*, *J. Cosmology Astropart. Phys.* **2025** (2025) 028 [2411.12022].
 - [4] A.G. Riess, W. Yuan, L.M. Macri, D. Scolnic, D. Brout, S. Casertano et al., *A Comprehensive Measurement of the Local Value of the Hubble Constant with $1 \text{ km s}^{-1} \text{ Mpc}^{-1}$ Uncertainty from the Hubble Space Telescope and the SH0ES Team*, *ApJ* **934** (2022) L7 [2112.04510].
 - [5] DESI Collaboration, A.G. Adame, J. Aguilar, S. Ahlen, S. Alam, D.M. Alexander et al., *DESI 2024 III: baryon acoustic oscillations from galaxies and quasars*, *J. Cosmology Astropart. Phys.* **2025** (2025) 012 [2404.03000].
 - [6] DESI Collaboration, M. Abdul-Karim, J. Aguilar, S. Ahlen, S. Alam, L. Allen et al., *DESI DR2 Results II: Measurements of Baryon Acoustic Oscillations and Cosmological Constraints*, *arXiv e-prints* (2025) arXiv:2503.14738 [2503.14738].
 - [7] E. Di Valentino, O. Mena, S. Pan, L. Visinelli, W. Yang, A. Melchiorri et al., *In the realm of the Hubble tension—a review of solutions*, *Classical and Quantum Gravity* **38** (2021) 153001 [2103.01183].
 - [8] G. Efstathiou, *A Lockdown Perspective on the Hubble Tension (with comments from the SH0ES team)*, *arXiv e-prints* (2020) arXiv:2007.10716 [2007.10716].
 - [9] W.L. Freedman, B.F. Madore, T.J. Hoyt, I.S. Jang, A.J. Lee and K.A. Owens, *Status Report on the Chicago-Carnegie Hubble Program (CCHP): Measurement of the Hubble Constant Using the Hubble and James Webb Space Telescopes*, *ApJ* **985** (2025) 203 [2408.06153].
 - [10] A.G. Riess, D. Scolnic, G.S. Anand, L. Breuval, S. Casertano, L.M. Macri et al., *JWST Validates HST Distance Measurements: Selection of Supernova Subsample Explains Differences in JWST Estimates of Local H_0* , *ApJ* **977** (2024) 120 [2408.11770].
 - [11] S. Birrer, A.J. Shajib, A. Galan, M. Millon, T. Treu, A. Agnello et al., *TDCOSMO. IV. Hierarchical time-delay cosmography - joint inference of the Hubble constant and galaxy density profiles*, *A&A* **643** (2020) A165 [2007.02941].
 - [12] B.P. Abbott, R. Abbott, T.D. Abbott, F. Acernese, K. Ackley, C. Adams et al., *A gravitational-wave standard siren measurement of the Hubble constant*, *Nature* **551** (2017) 85 [1710.05835].
 - [13] K. Hotokezaka, E. Nakar, O. Gottlieb, S. Nissanke, K. Masuda, G. Hallinan et al., *A Hubble constant measurement from superluminal motion of the jet in GW170817*, *Nature Astronomy* **3** (2019) 940 [1806.10596].
 - [14] Y.-Y. Wang, S.-P. Tang, Z.-P. Jin and Y.-Z. Fan, *The Late Afterglow of GW170817/GRB 170817A: A Large Viewing Angle and the Shift of the Hubble Constant to a Value More Consistent with the Local Measurements*, *ApJ* **943** (2023) 13 [2208.09121].
 - [15] A. Palmese, R. Kaur, A. Hajela, R. Margutti, A. McDowell and A. MacFadyen, *Standard siren measurement of the Hubble constant using GW170817 and the latest observations of the electromagnetic counterpart afterglow*, *Phys. Rev. D* **109** (2024) 063508 [2305.19914].
 - [16] L. Knox and M. Millea, *Hubble constant hunter's guide*, *Phys. Rev. D* **101** (2020) 043533 [1908.03663].
 - [17] T. Karwal and M. Kamionkowski, *Dark energy at early times, the hubble parameter, and the string axiverse*, *Phys. Rev. D* **94** (2016) 103523.
 - [18] V. Poulin, T.L. Smith, T. Karwal and M. Kamionkowski, *Early dark energy can resolve the hubble tension*, *Phys. Rev. Lett.* **122** (2019) 221301.
 - [19] F. Niedermann and M.S. Sloth, *Resolving the Hubble tension with new early dark energy*, *Phys. Rev. D* **102** (2020) 063527 [2006.06686].
 - [20] M. Braglia, M. Ballardini, W.T. Emond, F. Finelli, A.E. Gümrükçüoğlu, K. Koyama et al., *Larger value for H_0 by an evolving gravitational constant*, *Phys. Rev. D* **102** (2020) 023529 [2004.11161].
 - [21] G.P. Lynch, L. Knox and J. Chluba, *DESI observations and the Hubble tension in light of modified recombination*, *Phys. Rev. D* **110** (2024) 083538 [2406.10202].
 - [22] S.H. Mirpoorian, K. Jedamzik and L. Pogosian, *Modified recombination and the Hubble tension*, *Phys. Rev. D* **111** (2025) 083519 [2411.16678].
 - [23] K. Jedamzik and L. Pogosian, *Relieving the Hubble Tension with Primordial Magnetic Fields*, *Phys. Rev. Lett.* **125** (2020) 181302 [2004.09487].
 - [24] N. Schöneberg and L. Vacher, *The mass effect — variations of the electron mass and their impact on cosmology*, *J. Cosmology Astropart. Phys.* **2025** (2025)
-
- ³ <https://desilike.readthedocs.io/en/latest/>
- ⁴ <https://github.com/ashleyjross/BAOfit>

- 004 [2407.16845].
- [25] N. Schöneberg, G.F. Abellán, A.P. Sánchez, S.J. Witte, V. Poulin and J. Lesgourgues, *The H_0 Olympics: A fair ranking of proposed models*, *Phys. Rep.* **984** (2022) 1 [2107.10291].
- [26] E.J. Baxter and B.D. Sherwin, *Determining the Hubble constant without the sound horizon scale: measurements from CMB lensing*, *MNRAS* **501** (2021) 1823 [2007.04007].
- [27] O.H.E. Philcox, B.D. Sherwin, G.S. Farren and E.J. Baxter, *Determining the Hubble constant without the sound horizon: Measurements from galaxy surveys*, *Phys. Rev. D* **103** (2021) 023538 [2008.08084].
- [28] O.H.E. Philcox, G.S. Farren, B.D. Sherwin, E.J. Baxter and D.J. Brout, *Determining the Hubble constant without the sound horizon: A 3.6 % constraint on H_0 from galaxy surveys, CMB lensing, and supernovae*, *Phys. Rev. D* **106** (2022) 063530 [2204.02984].
- [29] G.S. Farren, O.H.E. Philcox and B.D. Sherwin, *Determining the Hubble constant without the sound horizon: Perspectives with future galaxy surveys*, *Phys. Rev. D* **105** (2022) 063503 [2112.10749].
- [30] M.S. Madhavacheril, F.J. Qu, B.D. Sherwin, N. MacCrann, Y. Li, I. Abril-Cabezas et al., *The Atacama Cosmology Telescope: DR6 Gravitational Lensing Map and Cosmological Parameters*, *ApJ* **962** (2024) 113 [2304.05203].
- [31] G.S. Farren, A. Krolewski, F.J. Qu, S. Ferraro, E. Calabrese, J. Dunkley et al., *Atacama Cosmology Telescope: Multiprobe cosmology with unWISE galaxies and ACT DR6 CMB lensing*, *Phys. Rev. D* **111** (2025) 083516 [2409.02109].
- [32] E.A. Zaborowski, P. Taylor, K. Honscheid, A. Cuceu, A. de Mattia, D. Huterer et al., *A Sound Horizon-Free Measurement of H_0 in DESI 2024*, *arXiv e-prints* (2024) arXiv:2411.16677 [2411.16677].
- [33] E.A. Zaborowski, P. Taylor, K. Honscheid, A. Cuceu, A. de Mattia, A. Krolewski et al., *H_0 Without the Sound Horizon (or Supernovae): A 2% Measurement in DESI DR1*, *arXiv e-prints* (2025) arXiv:2510.19149 [2510.19149].
- [34] S. Brieden, H. Gil-Marín and L. Verde, *A tale of two (or more) h 's*, *J. Cosmology Astropart. Phys.* **2023** (2023) 023 [2212.04522].
- [35] S. Brieden, H. Gil-Marín and L. Verde, *ShapeFit: extracting the power spectrum shape information in galaxy surveys beyond BAO and RSD*, *J. Cosmology Astropart. Phys.* **2021** (2021) 054 [2106.07641].
- [36] S. Brieden, H. Gil-Marín and L. Verde, *Model-agnostic interpretation of 10 billion years of cosmic evolution traced by BOSS and eBOSS data*, *J. Cosmology Astropart. Phys.* **2022** (2022) 024 [2204.11868].
- [37] B. Bahr-Kalus, D. Parkinson and E.-M. Mueller, *Measurement of the matter-radiation equality scale using the extended baryon oscillation spectroscopic survey quasar sample*, *MNRAS* **524** (2023) 2463 [2302.07484].
- [38] J.C. Hill, E. McDonough, M.W. Toomey and S. Alexander, *Early dark energy does not restore cosmological concordance*, *Phys. Rev. D* **102** (2020) 043507 [2003.07355].
- [39] T.L. Smith, V. Poulin and T. Simon, *Assessing the robustness of sound horizon-free determinations of the Hubble constant*, *Phys. Rev. D* **108** (2023) 103525 [2208.12992].
- [40] J.A. Kable and V. Miranda, *Sound horizon independent constraints on early dark energy: the role of supernova data*, *J. Cosmology Astropart. Phys.* **2024** (2024) 011 [2403.11916].
- [41] A. Krolewski and W.J. Percival, *Measuring the baryon fraction using galaxy clustering*, *Phys. Rev. D* **111** (2025) 063526 [2403.19236].
- [42] A. Krolewski, W.J. Percival and A. Woodfinden, *New Method to Determine the Hubble Parameter from Cosmological Energy-Density Measurements*, *Phys. Rev. Lett.* **134** (2025) 101002 [2403.19227].
- [43] A. Crespi, A. Krolewski and W. Percival, *Improving baryon fraction measurements from galaxy clustering: a consistent perturbation evolution approach*, , in preparation (2025) .
- [44] DESI Collaboration, A. Aghamousa, J. Aguilar, S. Ahlen, S. Alam, L.E. Allen et al., *The DESI Experiment Part I: Science, Targeting, and Survey Design*, *arXiv e-prints* (2016) arXiv:1611.00036 [1611.00036].
- [45] DESI Collaboration, A. Aghamousa, J. Aguilar, S. Ahlen, S. Alam, L.E. Allen et al., *The DESI Experiment Part II: Instrument Design*, *arXiv e-prints* (2016) arXiv:1611.00037 [1611.00037].
- [46] E.F. Schlafly, D. Kirkby, D.J. Schlegel, A.D. Myers, A. Raichoor, K. Dawson et al., *Survey Operations for the Dark Energy Spectroscopic Instrument*, *AJ* **166** (2023) 259 [2306.06309].
- [47] C. Poppett, L. Tyas, J. Aguilar, C. Bebek, D. Bramall, T. Claybaugh et al., *Overview of the Fiber System for the Dark Energy Spectroscopic Instrument*, *AJ* **168** (2024) 245.
- [48] J.H. Silber, P. Fagrelus, K. Fanning, M. Schubnell, J.N. Aguilar, S. Ahlen et al., *The Robotic Multiobject Focal Plane System of the Dark Energy Spectroscopic Instrument (DESI)*, *AJ* **165** (2023) 9 [2205.09014].
- [49] T.N. Miller, P. Doel, G. Gutierrez, R. Besuner, D. Brooks, G. Gallo et al., *The Optical Corrector for the Dark Energy Spectroscopic Instrument*, *AJ* **168** (2024) 95 [2306.06310].
- [50] DESI Collaboration, B. Abareshi, J. Aguilar, S. Ahlen, S. Alam, D.M. Alexander et al., *Overview of the Instrumentation for the Dark Energy Spectroscopic Instrument*, *AJ* **164** (2022) 207 [2205.10939].
- [51] J. Guy, S. Bailey, A. Kremin, S. Alam, D.M. Alexander, C. Allende Prieto et al., *The Spectroscopic Data Processing Pipeline for the Dark Energy Spectroscopic Instrument*, *AJ* **165** (2023) 144 [2209.14482].
- [52] A. Brodzeller, K. Dawson, S. Bailey, J. Yu, A.J. Ross, A. Bault et al., *Performance of the Quasar Spectral Templates for the Dark Energy Spectroscopic Instrument*, *AJ* **166** (2023) 66 [2305.10426].
- [53] DESI Collaboration, M. Abdul-Karim, A.G. Adame, D. Aguado, J. Aguilar, S. Ahlen et al., *Data Release 1 of the Dark Energy Spectroscopic Instrument*, *arXiv e-prints* (2025) arXiv:2503.14745 [2503.14745].
- [54] A.J. Ross, J. Aguilar, S. Ahlen, S. Alam, A. Anand, S. Bailey et al., *The construction of large-scale structure catalogs for the Dark Energy Spectroscopic Instrument*, *J. Cosmology Astropart. Phys.* **2025** (2025) 125 [2405.16593].

- [55] DESI Collaboration, A.G. Adame, J. Aguilar, S. Ahlen, S. Alam, D.M. Alexander et al., *DESI 2024 V: Full-Shape Galaxy Clustering from Galaxies and Quasars*, *arXiv e-prints* (2024) arXiv:2411.12021 [2411.12021].
- [56] M. Pinon, A. de Mattia, P. McDonald, E. Burtin, V. Ruhlmann-Kleider, M. White et al., *Mitigation of DESI fiber assignment incompleteness effect on two-point clustering with small angular scale truncated estimators*, *J. Cosmology Astropart. Phys.* **2025** (2025) 131 [2406.04804].
- [57] C.-H. Chuang, F.-S. Kitauro, F. Prada, C. Zhao and G. Yepes, *EZmocks: extending the Zel'dovich approximation to generate mock galaxy catalogues with accurate clustering statistics*, *MNRAS* **446** (2015) 2621 [1409.1124].
- [58] N. Findlay, S. Nadathur, W.J. Percival, A. de Mattia, P. Zarrouk, H. Gil-Marín et al., *Exploring HOD-dependent systematics for the DESI 2024 Full-Shape galaxy clustering analysis*, *J. Cosmology Astropart. Phys.* **2025** (2025) 007 [2411.12023].
- [59] DESI Collaboration, A.G. Adame, J. Aguilar, S. Ahlen, S. Alam, D.M. Alexander et al., *DESI 2024 IV: Baryon Acoustic Oscillations from the Lyman alpha forest*, *J. Cosmology Astropart. Phys.* **2025** (2025) 124 [2404.03001].
- [60] M. Rashkovetskyi, D.J. Eisenstein, J.N. Aguilar, D. Brooks, T. Claybaugh, S. Cole et al., *Validation of semi-analytical, semi-empirical covariance matrices for two-point correlation function for early DESI data*, *MNRAS* **524** (2023) 3894 [2306.06320].
- [61] DESI Collaboration, M. Abdul-Karim, J. Aguilar, S. Ahlen, S. Alam, L. Allen et al., *DESI DR2 Results II: Measurements of Baryon Acoustic Oscillations and Cosmological Constraints*, *arXiv e-prints* (2025) arXiv:2503.14738 [2503.14738].
- [62] L.H. Garrison, D.J. Eisenstein and P.A. Pinto, *A high-fidelity realization of the Euclid code comparison N-body simulation with ABACUS*, *MNRAS* **485** (2019) 3370 [1810.02916].
- [63] N.A. Maksimova, L.H. Garrison, D.J. Eisenstein, B. Hadzhiyska, S. Bose and T.P. Satterthwaite, *ABACUSSUMMIT: a massive set of high-accuracy, high-resolution N-body simulations*, *MNRAS* **508** (2021) 4017 [2110.11398].
- [64] J. Lasker, A. Carnero Rosell, A.D. Myers, A.J. Ross, D. Bianchi, M.M.S. Hanif et al., *Production of alternate realizations of DESI fiber assignment for unbiased clustering measurement in data and simulations*, *J. Cosmology Astropart. Phys.* **2025** (2025) 127 [2404.03006].
- [65] N. Schöneberg, *The 2024 BBN baryon abundance update*, *J. Cosmology Astropart. Phys.* **2024** (2024) 006 [2401.15054].
- [66] Particle Data Group, R.L. Workman, V.D. Burkert, V. Crede, E. Klempt, U. Thoma et al., *Review of Particle Physics*, *Progress of Theoretical and Experimental Physics* **2022** (2022) 083C01.
- [67] A.-K. Burns, T.M.P. Tait and M. Valli, *PRyMordial: the first three minutes, within and beyond the standard model*, *European Physical Journal C* **84** (2024) 86 [2307.07061].
- [68] S.-F. Chen, Z. Vlah and M. White, *Consistent modeling of velocity statistics and redshift-space distortions in one-loop perturbation theory*, *J. Cosmology Astropart. Phys.* **2020** (2020) 062 [2005.00523].
- [69] S.-F. Chen, Z. Vlah, E. Castorina and M. White, *Redshift-space distortions in Lagrangian perturbation theory*, *J. Cosmology Astropart. Phys.* **2021** (2021) 100 [2012.04636].
- [70] M. Bonici, G. D'Amico, J. Bel and C. Carbone, *Effort.jl: a fast and differentiable emulator for the Effective Field Theory of the Large Scale Structure of the Universe*, *JCAP* **09** (2025) 044 [2501.04639].
- [71] F. Schmidt, *Effect of relative velocity and density perturbations between baryons and dark matter on the clustering of galaxies*, *Phys. Rev. D* **94** (2016) 063508 [1602.09059].
- [72] S.-F. Chen, E. Castorina and M. White, *Biased tracers of two fluids in the Lagrangian picture*, *J. Cosmology Astropart. Phys.* **2019** (2019) 006 [1903.00437].
- [73] S.F. Chen, C. Howlett, M. White, P. McDonald, A.J. Ross, H.J. Seo et al., *Baryon acoustic oscillation theory and modelling systematics for the DESI 2024 results*, *MNRAS* **534** (2024) 544 [2402.14070].
- [74] B. Wallisch, *Cosmological probes of light relics*, Ph.D. thesis, University of Cambridge, UK, Jan., 2018.
- [75] J. Hamann, *Evidence for extra radiation? Profile likelihood versus Bayesian posterior*, *J. Cosmology Astropart. Phys.* **2012** (2012) 021 [1110.4271].
- [76] T. Simon, P. Zhang, V. Poulin and T.L. Smith, *Consistency of effective field theory analyses of the BOSS power spectrum*, *Phys. Rev. D* **107** (2023) 123530 [2208.05929].
- [77] P. Carrilho, C. Moretti and A. Pourtsidou, *Cosmology with the EFTofLSS and BOSS: dark energy constraints and a note on priors*, *J. Cosmology Astropart. Phys.* **2023** (2023) 028 [2207.14784].
- [78] M. Maus, Y. Lai, H.E. Noriega, S. Ramirez-Solano, A. Aviles, S. Chen et al., *A comparison of effective field theory models of redshift space galaxy power spectra for DESI 2024 and future surveys*, *J. Cosmology Astropart. Phys.* **2025** (2025) 134 [2404.07272].
- [79] H. Zhang, M. Bonici, G. D'Amico, S. Paradiso and W.J. Percival, *HOD-informed prior for EFT-based full-shape analyses of LSS*, *J. Cosmology Astropart. Phys.* **2025** (2025) 041 [2409.12937].
- [80] M.M. Ivanov, C. Cuesta-Lazaro, S. Mishra-Sharma, A. Obuljen and M.W. Toomey, *Full-shape analysis with simulation-based priors: Constraints on single field inflation from BOSS*, *Phys. Rev. D* **110** (2024) 063538 [2402.13310].
- [81] M.M. Ivanov, A. Obuljen, C. Cuesta-Lazaro and M.W. Toomey, *Full-shape analysis with simulation-based priors: Cosmological parameters and the structure growth anomaly*, *Phys. Rev. D* **111** (2025) 063548 [2409.10609].
- [82] H. Zhang, M. Bonici, A. Rocher, W.J. Percival, A. de Mattia, J.N. Aguilar et al., *Enhancing DESI DR1 Full-Shape analyses using HOD-informed priors*, *arXiv e-prints* (2025) arXiv:2504.10407 [2504.10407].
- [83] M.D. Hoffman and A. Gelman, *The No-U-Turn sampler: adaptively setting path lengths in Hamiltonian Monte Carlo*, *J. Mach. Learn. Res.* **15** (2014) 1593.
- [84] Z. Ding, H.-J. Seo, Z. Vlah, Y. Feng, M. Schmittfull and F. Beutler, *Theoretical systematics of Future Baryon Acoustic Oscillation Surveys*, *MNRAS* **479**

- (2018) 1021 [1708.01297].
- [85] M. White, *Reconstruction within the Zeldovich approximation*, *MNRAS* **450** (2015) 3822 [1504.03677].
- [86] X. Chen, Z. Ding, E. Paillas, S. Nadathur, H. Seo, S. Chen et al., *Extensive analysis of reconstruction algorithms for DESI 2024 baryon acoustic oscillations*, *arXiv e-prints* (2024) arXiv:2411.19738 [2411.19738].
- [87] E. Paillas, Z. Ding, X. Chen, H. Seo, N. Padmanabhan, A. de Mattia et al., *Optimal reconstruction of baryon acoustic oscillations for DESI 2024*, *J. Cosmology Astropart. Phys.* **2025** (2025) 142 [2404.03005].
- [88] N. Padmanabhan, X. Xu, D.J. Eisenstein, R. Scalzo, A.J. Cuesta, K.T. Mehta et al., *A 2 per cent distance to $z = 0.35$ by reconstructing baryon acoustic oscillations - I. Methods and application to the Sloan Digital Sky Survey*, *MNRAS* **427** (2012) 2132 [1202.0090].
- [89] E. Camphuis, W. Quan, L. Balkenhol, A.R. Khalife, F. Ge, F. Guidi et al., *SPT-3G D1: CMB temperature and polarization power spectra and cosmology from 2019 and 2020 observations of the SPT-3G Main field*, *arXiv e-prints* (2025) arXiv:2506.20707 [2506.20707].
- [90] S.-F. Chen and M. Zaldarriaga, *It's all Ok: curvature in light of BAO from DESI DR2*, *J. Cosmology Astropart. Phys.* **2025** (2025) 014 [2505.00659].
- [91] H. García Escudero, S. Hamidreza Mirpoorian and L. Pogorian, *Sound-Horizon-Agnostic Inference of the Hubble Constant and Neutrino Mass from BAO, CMB Lensing, and Galaxy Weak Lensing and Clustering*, *arXiv e-prints* (2025) arXiv:2509.16202 [2509.16202].
- [92] A. Lewis, *GetDist: a Python package for analysing Monte Carlo samples*, *J. Cosmology Astropart. Phys.* **2025** (2025) 025 [1910.13970].
- [93] A. Pal, *Lux: Explicit Parameterization of Deep Neural Networks in Julia*, Apr., 2023. 10.5281/zenodo.7808903.
- [94] T.E. Fjelde, K. Xu, D. Widmann, M. Tarek, C. Pfiffer, M. Trapp et al., *Turing.jl: a general-purpose probabilistic programming language*, *ACM Trans. Probab. Mach. Learn.* (2025) .
- [95] H. Ge, K. Xu and Z. Ghahramani, *Turing: A language for flexible probabilistic inference*, in *Proceedings of the Twenty-First International Conference on Artificial Intelligence and Statistics*, A. Storkey and F. Perez-Cruz, eds., vol. 84 of *Proceedings of Machine Learning Research*, pp. 1682–1690, PMLR, 09–11 Apr, 2018, <https://proceedings.mlr.press/v84/ge18b.html>.
- [96] A. Chudaykin, M.M. Ivanov, O.H.E. Philcox and M. Simonović, *Nonlinear perturbation theory extension of the Boltzmann code CLASS*, *Phys. Rev. D* **102** (2020) 063533 [2004.10607].
- [97] D. Tsaliakhovich and C. Hirata, *Relative velocity of dark matter and baryonic fluids and the formation of the first structures*, *Phys. Rev. D* **82** (2010) 083520 [1005.2416].
- [98] A. Barreira, G. Cabass, D. Nelson and F. Schmidt, *Baryon-CDM isocurvature galaxy bias with IllustrisTNG*, *J. Cosmology Astropart. Phys.* **2020** (2020) 005 [1907.04317].
- [99] H. Khoraminezhad, T. Lazeyras, R.E. Angulo, O. Hahn and M. Viel, *Quantifying the impact of baryon-CDM perturbations on halo clustering and baryon fraction*, *J. Cosmology Astropart. Phys.* **2021** (2021) 023 [2011.01037].
- [100] J. Yoo, N. Dalal and U. Seljak, *Supersonic relative velocity effect on the baryonic acoustic oscillation measurements*, *J. Cosmology Astropart. Phys.* **2011** (2011) 018 [1105.3732].
- [101] J.A. Blazek, J.E. McEwen and C.M. Hirata, *Streaming Velocities and the Baryon Acoustic Oscillation Scale*, *Phys. Rev. Lett.* **116** (2016) 121303 [1510.03554].
- [102] J. Yoo and U. Seljak, *Signatures of first stars in galaxy surveys: Multitracer analysis of the supersonic relative velocity effect and the constraints from the BOSS power spectrum measurements*, *Phys. Rev. D* **88** (2013) 103520 [1308.1401].
- [103] F. Beutler, U. Seljak and Z. Vlah, *Constraining the relative velocity effect using the Baryon Oscillation Spectroscopic Survey*, *MNRAS* **470** (2017) 2723 [1612.04720].
- [104] Z. Slepian, D.J. Eisenstein, J.A. Blazek, J.R. Brownstein, C.-H. Chuang, H. Gil-Marín et al., *Constraining the baryon-dark matter relative velocity with the large-scale three-point correlation function of the SDSS BOSS DR12 CMASS galaxies*, *MNRAS* **474** (2018) 2109 [1607.06098].
- [105] O.H.E. Philcox and M.M. Ivanov, *BOSS DR12 full-shape cosmology: A CDM constraints from the large-scale galaxy power spectrum and bispectrum monopole*, *Phys. Rev. D* **105** (2022) 043517 [2112.04515].
- [106] M. Maus, S. Chen, M. White, J. Aguilar, S. Ahlen, A. Aviles et al., *An analysis of parameter compression and Full-Modeling techniques with Velocileptors for DESI 2024 and beyond*, *J. Cosmology Astropart. Phys.* **2025** (2025) 138 [2404.07312].

Appendix A: Impact of relative velocity

Besides perturbations in the total combined density of baryons and dark matter, galaxy clustering can also respond to relative perturbations in the density and velocity of baryons and dark matter [71–73]. These relative perturbations grow much slower than the standard adiabatic growing mode, but they have a larger imprint of the BAO feature and hence are a potential source of systematic error for this work. At linear order, the relative density perturbations decouple from the matter perturbations and grow as [71]

$$\delta_{bc}(a) = R_+ + R_- D_{bc}(a) \quad (\text{A1})$$

where R_+ and R_- are constant in redshift and

$$D_{bc} = \int_{\ln a}^{\infty} \frac{d \ln a'}{a'^2 H(a')/H_0} \quad (\text{A2})$$

The solution for relative density perturbations thus consists of two modes, one that is a constant compensated perturbation where δ_c and δ_b oppose each other, and another decaying mode that arises from the initial relative velocity, v_{bc} , which decays as $1/a$:

$$R_- = \frac{\theta_{bc}(z=0)}{H_0} \quad (\text{A3})$$

where θ_{bc} is the divergence of the relative velocity. The linear evolution of δ_{bc} and θ_{bc} can therefore be computed from the transfer functions $T_b(k)$, $T_c(k)$. $R_-(k)$ and $R_+(k)$ are therefore given by

$$R_-(k) = \frac{k}{H_0} \frac{T_{vbc}(k)}{T_m(k)} \delta_m(k, z=0) \quad (A4)$$

$$R_+(k) = \frac{T_b(k) - T_c(k)}{T_m(k)} \delta_m(k, 0) - R_-(k) D_{bc}(z=0) \quad (A5)$$

where the second term is $\sim 1\%$ of the first term.

The dominant contributions to the galaxy power spectrum are the cross-terms, $b_1 b_{\delta_{bc}} P_{\delta_{bc}\delta}(k)$ and $b_1 b_{v_{bc}^2} P_{v_{bc}^2\delta}(k)$ [73]. Because θ_{bc} is much smaller than δ_{bc} , the $P_{\theta_{bc}\delta}$ term is suppressed. The $P_{v_{bc}^2\delta}$ is the relative velocity effect from [97] arising from supersonic baryon-dark matter velocities. While it is a one-loop rather than linear order term, it can be enhanced by the rms fluctuation of the relative velocities, σ_{bc} , $\sim 30 \text{ km s}^{-1}$ at recombination.

The relative velocity terms affect both the amplitude and position of the BAO peak. Their impact on the BAO peak position was shown to be small relative to the DESI DR1 errors in [73], and also small relative to the final expected errors from DESI. We will perform a similar analysis to estimate the impact of the relative velocity errors on γ_b .

A full treatment of these terms at one-loop order in the post-reconstruction redshift-space power spectrum is challenging (see [71, 72] for the pre-reconstruction redshift space power spectrum in perturbation theory). We therefore proceed with an approximate treatment in which we add $P_{\delta_{bc}\delta}$ and $P_{v_{bc}^2\delta}$ to a noiseless mock, fit the BAO amplitude in our baseline model, and measure the shift in γ_b . We use an approximate damping model to propagate leading-order templates for $P_{\delta_{bc}\delta}$ (linear-order) and $P_{v_{bc}^2\delta}$ (one-loop) to the nonlinear, post-reconstruction field. We defer improvements in this modelling to future work in which we aim to jointly fit γ_b , $b_{\delta_{bc}}$, and $b_{v_{bc}^2}$. In this approximate model, the contributions of $P_{\delta_{bc}\delta}$ and $P_{v_{bc}^2\delta}$ take the form:

$$P_{\delta_{bc}\delta}^{\text{NL, recon}}(k, \mu) = 2(b_1 + f\mu^2) b_{\delta_{bc}} P_{\delta_{bc}\delta}(k, z=0) D(z) \times \exp\left(-0.5k^2 \left[(1-\mu^2)\Sigma_{\perp}^2 + \mu^2\Sigma_{\parallel}^2\right]\right) \left(\frac{1}{1 + 0.5k^2\mu^2\Sigma_{\text{fog}}^2}\right)^2 \quad (A6)$$

$$P_{v_{bc}^2\delta}^{\text{NL, recon}}(k, \mu) = (b_1 + f\mu^2) b_{v_{bc}^2} P_{v_{bc}^2\delta}(k, z=0) D^2(z) \times \exp\left(-0.5k^2 \left[(1-\mu^2)\Sigma_{\perp}^2 + \mu^2\Sigma_{\parallel}^2\right]\right) \left(\frac{1}{1 + 0.5k^2\mu^2\Sigma_{\text{fog}}^2}\right)^2 \quad (A7)$$

where the linear and one-loop calculations of $P_{\delta_{bc}\delta}$ and $P_{v_{bc}^2\delta}$ are from [73]. The scaling with the growth factor is different: for $P_{\delta_{bc}\delta}$, δ grows with $D(z)$ but δ_{bc} is constant, causing the power spectrum to scale with only a single power of the growth factor. For $P_{v_{bc}^2\delta}$, v_{bc}^2 is constant in redshift but the leading contribution is at one-loop order, hence leading to two powers of the growth factor. Rather than split $P_{\delta_{bc}\delta}$ and $P_{v_{bc}^2\delta}$ into wiggle and no-wiggle components, we damp the entire power spectrum. This suppresses the amplitude of the no-wiggle component, but the dominant impact on the observed power spectrum comes from the oscillatory part, with $< 1\%$ contribution from the broadband. Our results are therefore minimally affected by the extra damping on the broadband component. In Fig. 8, we show the contributions from $P_{\delta_{bc}\delta}$ and $P_{v_{bc}^2\delta}$ to the galaxy power spectrum.

The impact of these terms depends on the unknown bias coefficients, $b_{\delta_{bc}}$ and $b_{v_{bc}^2}$. For galaxies with a similar stellar mass to DESI and BOSS, [98] measures $b_{\delta_{bc}}$ using the separate-universe technique in hydrodynamical simulations and finds $|b_{\delta_{bc}}| \sim 0.5$, with an increasing trend towards higher halo masses and redshifts. Similarly, [99] finds $b_{\delta_{bc}} \sim -0.4$ for BOSS-like galaxies using separate-universe N -body simulations. The relative velocity bias is more poorly estimated, ranging between $10^{-5} \sigma_{bc}^{-2}$ to $0.01 \sigma_{bc}^{-2}$ [71, 100, 101]. Unless galaxy formation preserves significant memory of early times, smaller values of $b_{v_{bc}^2}$ are more likely [102]. We therefore assume a fiducial value of $b_{v_{bc}^2} = 10^{-3} \sigma_{bc}^{-2}$.

We measure γ_b from the mock datasets with relative density and velocity perturbations using the post-reconstruction fits, and find

$$\Delta\gamma_b = -0.0040 \left(\frac{b_{\delta_{bc}}}{0.5}\right) \quad (A8)$$

$$\Delta\gamma_b = -0.0015 \left(\frac{b_{v_{bc}^2}}{10^{-3}}\right) \quad (A9)$$

This is at most 0.40σ for $b_{\delta_{bc}}$, justifying our decision to neglect these terms in our fits. However, for future datasets with higher precision, we will be required to marginalize over these terms. The sizes of these biases can be constrained by their impact on the power spectrum broadband in full-shape fits [101, 103, 104] and indeed BOSS is already nearly large enough to constrain $b_{v_{bc}^2}$ [103].

Appendix B: Comparison to previous baryon fraction fitting methodology

In this section, we compare our baseline method, using [43] to define γ_b directly in CAMB, to our old fitting method used in the BOSS analysis [41], in which we split the transfer function into baryonic and CDM components.

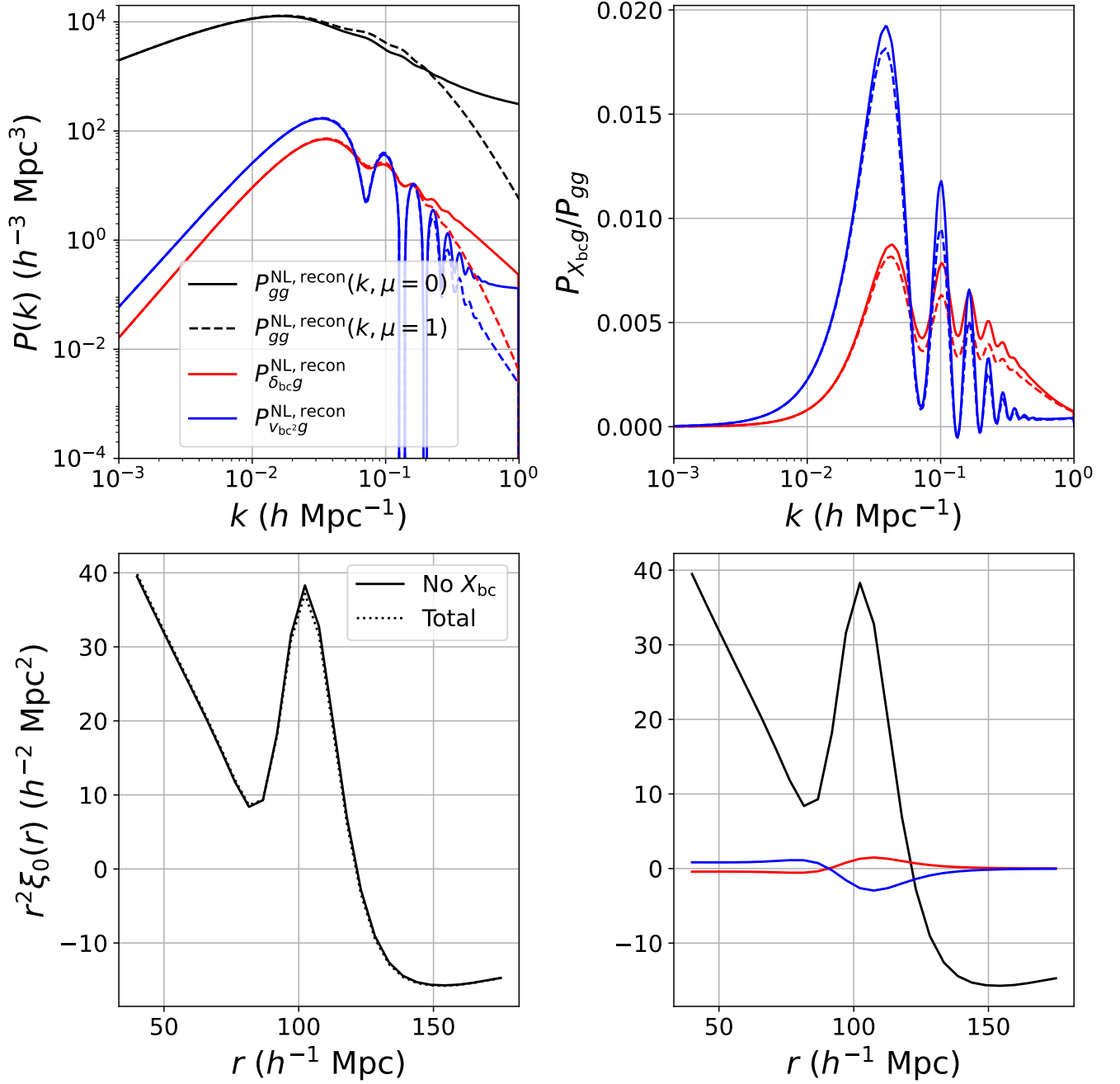


FIG. 8. Contributions of relative density and velocity terms to the galaxy power spectrum. *Top left:* Black shows the power spectrum without relative velocity and density terms; red shows the contribution from the galaxy-relative density δ_{bc} term (fiducial value of $b_{\delta_{bc}} = 0.5$); and blue shows the contribution from the galaxy-streaming velocity dispersion v_{bc}^2 term ($b_{v_{bc}^2} = 0.01\sigma_{bc}^{-2}$, 10 times larger than the fiducial value for ease of display). Solid lines are for $\mu = 0$ and dashed lines for $\mu = 1$, using the approximate exponential model to relate the leading-order templates for $P_{\delta_{bc},\delta}$ and $P_{v_{bc}^2,\delta}$ to the post-reconstruction nonlinear power spectrum. *Top right:* Fractional contribution of $P_{\delta_{bc},\delta}$ and $P_{v_{bc}^2,\delta}$ to the total power spectrum. *Bottom left:* Correlation function monopole for both the total power spectrum (dashed) and the galaxy density terms only (solid), using the fiducial values of $b_{\delta_{bc}} = 0.5$ and $b_{v_{bc}^2} = 0.001\sigma_{bc}^{-2}$. *Bottom right:* Contributions of the $P_{\delta_{bc},\delta}$ and $P_{v_{bc}^2,\delta}$ terms ($b_{\delta_{bc}} = 0.5$ and $b_{v_{bc}^2} = 0.01\sigma_{bc}^{-2}$).

1. EFT priors in the CLASS-PT based pipeline

In [41], we used a different EFT code (CLASS-PT), whereas we now use **Velocileptors**, to match the default code used in the DESI full-shape analysis [55]. In order to consider the impact of this choice, we need to match the priors adopted for the CLASS-PT based analysis to those we now adopt using **Velocileptors**.

In the CLASS-PT bias basis (“East Coast” basis), there are 11 free nuisance parameters per tracer (4 biases $b_1, b_2, b_{\mathcal{G}_2}, b_{\Gamma_3}$, 4 counterterms c_0, c_2, c_4, \tilde{c} , and 3 stochastic parameters $P_{\text{shot}}, a_0, a_2$). The priors used in [41] are shown in Table V. These are very similar to the priors used in [105], except that we halve the width of the priors on the counterterms and stochastic parameters to reduce prior volume effects. We refer to these as the “BOSS priors.”

While these priors were sufficient for recovering unbiased cosmology on BOSS mocks and noiseless theory vectors using the BOSS covariance, we find that the prior volume effects are more severe on DESI data and these priors are no longer sufficient. To recover unbiased cosmology with the “old” pipeline, we therefore use a set of priors derived from translating the DESI priors to the East Coast basis. These priors are not identical to the DESI priors, because they are defined in a different basis so the volume measure is different, but we instead match the prior widths on each parameter individually.

The DESI priors are defined in terms of Lagrangian bias parameters. These can be translated to the Eulerian bias parameters used by CLASS-PT:

$$b_2^E = b_2^L + \frac{8}{21}b_1^L \quad (\text{B1})$$

$$b_{\mathcal{G}_2}^E = b_s^L - \frac{2}{7}b_1^L \quad (\text{B2})$$

In the DESI full-shape analysis, the following priors are applied to the bias parameters:

$$(1 + b_1^L)\sigma_8(z) \rightarrow U(0, 3) \quad (\text{B3})$$

$$b_2^L\sigma_8(z)^2 \rightarrow N(0, 5^2) \quad (\text{B4})$$

$$b_s^L\sigma_8(z)^2 \rightarrow N(0, 5^2) \quad (\text{B5})$$

We can then express the prior on $b_2^E, \sigma_{b_2^E}$ using error propagation:

$$\sigma_{b_2^E\sigma_8(z)^2}^2 = \sigma_{b_2^L\sigma_8(z)^2}^2 + \left(\frac{8}{21}\right)^2 \sigma_8(z)^2 \sigma_{b_1^L\sigma_8(z)}^2 \quad (\text{B6})$$

The standard deviation of the uniform distribution between 0 and 3 is 0.87, while the standard deviation of $b_2^L\sigma_8(z)^2$ is 5. Hence the second term is $\sim 0.3\%$ of the first term at $z = 0$ and smaller at higher redshift. Likewise, the second term only shifts the mean of $b_2^E\sigma_8(z)^2$ by

~ 0.2 at $z = 0$, tiny compared to the width of the prior. Hence the prior on b_2^E can be approximated by:

$$b_2^E\sigma_8(z)^2 \rightarrow N(0, 5^2) \quad (\text{B7})$$

Similarly, for $b_{\mathcal{G}_2}^E$, the second term is $\sim 0.2\%$ of the first term, and the prior is also the same as on b_s^L :

$$b_{\mathcal{G}_2}^E\sigma_8(z)^2 \rightarrow N(0, 5^2) \quad (\text{B8})$$

Finally, in the DESI prior basis, the third-order bias is set to zero, hence we fix b_{Γ_3} to zero.

The counterterm priors are set by specifying that the counterterm contribution to the power spectrum is at most $0.5\times$ linear theory. The CLASS-PT counterterm contribution is given by:

$$P_{\text{ctr}}^{\text{CLASS-PT}} = -2\tilde{c}_0k^2P_{\text{lin}}(k) - 2\tilde{c}_2f\mu^2k^2P_{\text{lin}}(k) - 2\tilde{c}_4f^2\mu^4k^2P_{\text{lin}}(k) - \tilde{c}(z)f^4\mu^4k^4(b_1 + f\mu^2)^2P_{\text{lin}}(k) \quad (\text{B9})$$

where the basis $\tilde{c}_0, \tilde{c}_2, \tilde{c}_4$ is rotated into the basis c_0, c_2, c_4 on which the prior is defined:

$$c_0 = \tilde{c}_0 + \frac{f}{3}\tilde{c}_2 + \frac{f^2}{5}\tilde{c}_4 \quad (\text{B10})$$

$$c_2 = \tilde{c}_2 + \frac{6f}{7}\tilde{c}_4 \quad (\text{B11})$$

$$c_4 = \tilde{c}_4 \quad (\text{B12})$$

The linear contribution to the power spectrum is:

$$P_{\text{lin cont.}} = (b_1^E + f\mu^2)^2P_{\text{lin}}(k) \quad (\text{B13})$$

Since we are defining prior widths, we can ignore the overall negative sign in Eq. B9, and then by setting Eq. B9 and $0.5\times$ Eq. B13 equal order-by-order in μ , we obtain:

$$2\tilde{c}_0k^2 = 0.5(b_1^E)^2 \quad (\text{B14})$$

$$2\tilde{c}_2k^2 = b_1^E \quad (\text{B15})$$

Since we do not use the hexadecapole, we fix c_4 to zero (as in the DESI full-shape prior). We can then compute prior widths on c_0 and c_2 , adding the two terms in c_0 in quadrature since they are independent. We use the best-fit b_1^E from the DESI full-shape fits to Abacus and evaluate at the effective redshifts of the Abacus mocks (0.2, 0.5, 0.8, 0.8, 1.325, 1.4):

$$\frac{c_{0,i}}{(\text{Mpc}/h)^2} \sim \mathcal{N}(0, \sigma_{c_0,i}^2) \quad (\text{B16})$$

$$\sigma_{c_0} = [19.1, 25.5, 33.9, 34.5, 17.0, 35.2]$$

$$\frac{c_{2,i}}{(\text{Mpc}/h)^2} \sim \mathcal{N}(0, \sigma_{c_2,i}^2) \quad (\text{B17})$$

$$\sigma_{c_2} = [21.4, 24.7, 28.7, 28.9, 19.9, 29.2]$$

Parameter	BOSS prior	DESI prior, b^n basis
b_1	flat[0,4]	flat[0,4]
b_2	$\mathcal{N}(0, 1^2)$	$\mathcal{N}(0, 5^2)$
$b_{\mathcal{G}_2}$	$\mathcal{N}(0, 1^2)$	$\mathcal{N}(0, 5^2)$
b_{Γ_3}	$\mathcal{N}(\frac{23}{42}(b_1 - 1), 1^2)$	$\frac{23}{42}(b_1 - 1)$
c_0 [Mpc/h] ²	$\mathcal{N}(0, 15^2)$	$\mathcal{N}(0, \sigma_{c_0}^2), \sigma_{c_0} = [19.1, 25.5, 33.9, 34.5, 17.0, 35.2]$
c_2 [Mpc/h] ²	$\mathcal{N}(30, 15^2)$	$\mathcal{N}(0, \sigma_{c_0,i}^2), \sigma_{c_0} = [21.4, 24.7, 28.7, 28.9, 19.9, 29.2]$
c_4 [Mpc/h] ²	$\mathcal{N}(0, 15^2)$	0
\tilde{c} [Mpc/h] ⁴	$\mathcal{N}(500, 250^2)$	0
P_{shot}	$\mathcal{N}(0, 0.5^2)$	$\mathcal{N}(0, 2^2)$
a_0	$\mathcal{N}(0, 0.5^2)$	0
a_2	$\mathcal{N}(0, 0.5^2)$	$\mathcal{N}(0, \sigma_{a_2,i}^2), \sigma_{a_2} = [6.2, 6.2, 6.2, 6.2, 0.85, 0.99]$

TABLE V. Priors on Eulerian bias parameters, counterterms, and stochastic terms used when measuring γ_b using the CLASS-PT pipeline used in [41]. The prior used in that work (“BOSS prior”) is shown in the left column. The right column shows the best-validated prior for the DESI analysis using this pipeline. The widths of these priors are motivated to match the priors used in the DESI Full-Shape analysis [55], but we sample in the bias parameters rather than re-scaling them by powers of σ_8 to reduce projection effects in γ_b .

Since the \tilde{c} counterterm only affects the hexadecapole, it is also set to zero.

Finally, we translate the shot noise parameters, where the contributions to the stochastic terms are

$$P_{\text{sto}}^{\text{CLASS-PT}} = \frac{1}{\bar{n}} \left(P_{\text{shot}} + a_0 \left(\frac{k}{k_{\text{NL}}} \right)^2 + a_2 \mu^2 \left(\frac{k}{k_{\text{NL}}} \right)^2 \right) \quad (\text{B18})$$

and in **Velocileptors**

$$P_{\text{sto}}^{\text{vel.}} = \frac{1}{\bar{n}} (\text{SN}_0 + \text{SN}_2 \mu^2 k^2) \quad (\text{B19})$$

Hence, the prior on P_{shot} is the same as that on SN_0 :

$$P_{\text{shot}} \sim \mathcal{N}(0, 2^2) \quad (\text{B20})$$

and a_0 is fixed to zero since there is no $\propto \mu^0 k^2$ stochastic term in **Velocileptors**. The prior on SN_2 is

$$\text{SN}_2 \rightarrow \mathcal{N}(0, 5^2) \times f_{\text{sat}} \frac{\sigma_{\text{eff}}^2}{\bar{n}_g} \quad (\text{B21})$$

Using the satellite fractions and velocity dispersions from Table 2 in [106], we find

$$\begin{aligned} a_{2,i} &\sim \mathcal{N}(0, \sigma_{a_{2,i}}^2) \\ \sigma_{a_2} &= [6.2, 6.2, 6.2, 6.2, 0.85, 0.99] \end{aligned} \quad (\text{B22})$$

When applying these priors to ΛCDM constraints, we show in Fig. 9 that they lead to good consistency between our pipeline and the fiducial DESI full-shape results on Abacus mocks, with some minor differences in n_s and ω_{cdm} likely due to slight differences in perturbative expansions. Most notably, using the DESI bias basis and prior substantially mitigates the projection effects in σ_8 , reducing the $\sim 1\sigma$ bias on σ_8 with the CLASS-PT priors. The remaining differences in σ_8 disappear when the covariance is scaled down by a factor of 25 (approaching the maximum of the posterior in both the CLASS-PT and DESI runs).

2. Results on mocks

In Fig. 10, we compare parameters inferred from the Abacus mocks from our baseline pipeline from the main text of the paper to the CLASS-PT-based pipeline used in the previous analysis. We find that the DESI priors (defined in the $b_n \sigma_8^n$ basis) have large projection effects on h^{dens} and γ_b . These prior volume effects arise from the degeneracy between γ_b and σ_8 . The degeneracy is shown in Fig. 11, which compares the impact of changing σ_8 and γ_b on the model monopole and quadrupole. This arises from the suppression of the power spectrum on scales smaller than the baryonic Jeans scale. This degeneracy means that in the basis where the bias parameters are scaled by σ_8 , we make the rescaled bias parameters much more degenerate with γ_b , leading to dramatically worse prior volume effects on γ_b . We resolve this by using the DESI priors, but sampling in b_n , rather than $b_n \sigma_8^n$.

Apart from the DESI priors defined in the $b_n \sigma_8^n$ basis, the other three configurations produce consistent and unbiased constraints on h^{dens} and γ_b . In particular, the results using CLASS-PT and the priors from our BOSS analysis [41] are very similar to those using CLASS-PT and the DESI matched priors with the b_n basis. We also summarize these results in Table VI, which shows that for the CLASS-PT pipeline, the BOSS priors have worse projection effects on noiseless ΛCDM mocks than the DESI priors in the b_n basis. As a result, our default configuration in the CLASS-PT pipeline (which we also test on data) uses the DESI priors in the b_n basis.

The baseline constraints from the updated splitting method of [43] have slightly tighter constraints on γ_b and h_{dens} than the old $T(k)$ splitting method, since the new method essentially allows the baryon fraction to affect the baryon and CDM transfer functions. This allows the new method to consistently extract all of the baryon fraction information.

We also test the CLASS-PT pipeline (with the fiducial prior choice: DESI-matched priors with b_n basis) on

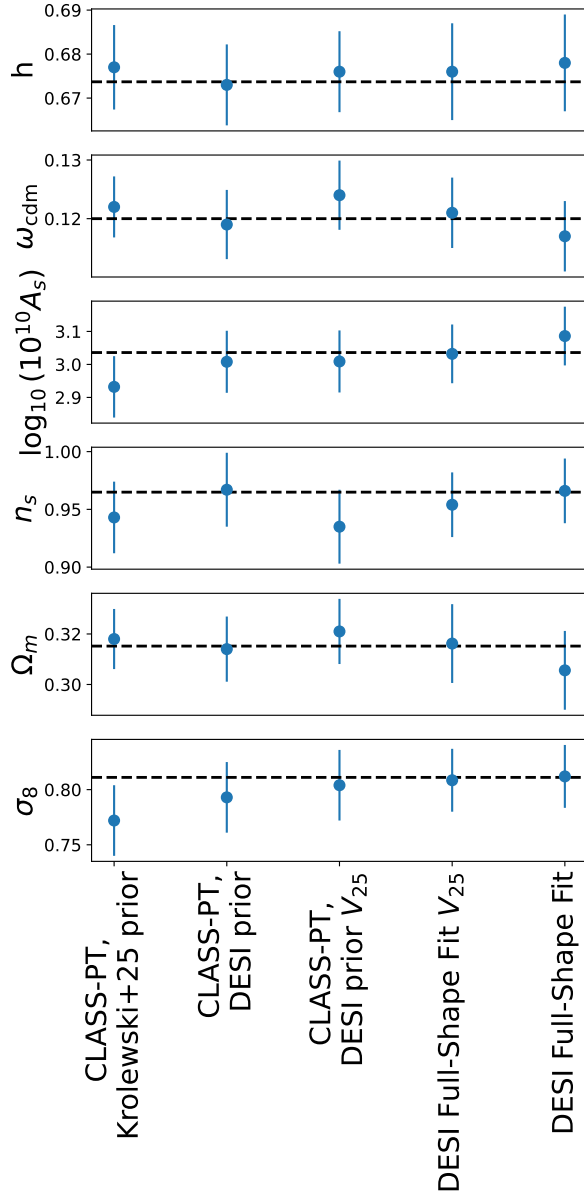


FIG. 9. Comparison of Λ CDM constraints between our pipeline and the DESI Full-Shape pipeline used in [55]. The left-most set of points comes from CLASS-PT run with the prior from Krolewski+25 [41] (very similar to the default CLASS-PT priors in [105]), fitting the mean of the 25 Abacus mocks and using the covariance matrix from the DESI data. The next set of points also uses CLASS-PT, but with a bias prior matching the choices of [55]. The third set uses the same fitting method as the second set, but scaling the covariance by a factor of 25 to appropriately match the fluctuations in the $25\times$ larger volume considered. The fourth and fifth points are taken from the DESI fits using Velocileptors and the nuisance parameter priors from Table 4 in [55], either using the DESI Y1 covariances (fifth column) or the covariance scaled down by 25 (fourth column).

noiseless mocks in Λ CDM and EDE with different true values of the baryon fraction. We find generally good recovery of the input parameters, with biases on f_b and h typically $< 0.5\sigma$ and similar performance on the Λ CDM and EDE mocks. These biases are somewhat larger than the $0.1\text{--}0.2\sigma$ biases found in our baseline method.

3. Results on data

In Fig. 12 and Table VII, we show that our results on data are robust to the method used to measure the baryon fraction from the full shape of the power spectrum. First, we find that variations in our baseline result do not change H_0 much; if we use the transfer function split to measure γ_b rather than the new approach of [43], H_0 drops by $0.3 \text{ km s}^{-1} \text{ Mpc}^{-1}$. If we also remove the HOD-informed prior, H_0 rises by $1.8 \text{ km s}^{-1} \text{ Mpc}^{-1}$. If we instead use the CLASS-PT pipeline with DESI priors (in the b_n basis where projection effects are minimized), we find a slightly higher H_0 , with a slightly larger errorbar, than the baseline results. Since this run uses Ly α BAO, we compare it to our baseline run including Ly α and find good consistency in Ω_m with a small offset in γ_b . All of these differences are consistent with noise fluctuations given the slightly different statistical power of each result. Moreover, the changes are at most 0.3σ , well within our statistical uncertainty on H_0 .

Appendix C: Detailed comparison of post-reconstruction fits to DESI baseline

In Table VIII, we compare the median of the 25 fits to the Abacus altmtl mocks between our pipeline to fit the BAO amplitude and the DESI baseline. Our pipeline has similar constraining power on α_{iso} and slightly worse constraining power on α_{AP} ; this is due to the extra free parameters and broader priors on the damping parameters in our pipeline vs. the DESI baseline.

In Table IX, we compare in more detail the offset between the two pipelines for LRG at $0.4 < z < 0.6$. The first three rows reproduce the columns of Table VIII, while the next rows show various other changes in the pipeline. The dominant changes driving the offset in α_{iso} ($\Delta\alpha_{\text{iso}} = 0.008$) are the larger fitting range in our fits ($\Delta\alpha_{\text{iso}} = 0.002$) and the fact that the baseline DESI fits sample in α_{iso} and α_{AP} rather than α_{\parallel} and α_{\perp} . The larger errors on α_{AP} are primarily driven by the extra freedom in our model, with broader priors on the damping parameters, extra α parameters changing the broadband, and varying γ_b and b_{∂} . These choices tighten α_{AP} constraints by $\sim 25\%$. Parameterizing the bias with b_1 and f , as in the DESI baseline (rather than B_0 and B_2 in our fits) further decreases the α_{AP} error by 5%. Offsets in α_{AP} are primarily driven by the nuisance parameter priors, and the basis to sample the α parameters, although there are also small shifts from the bias param-

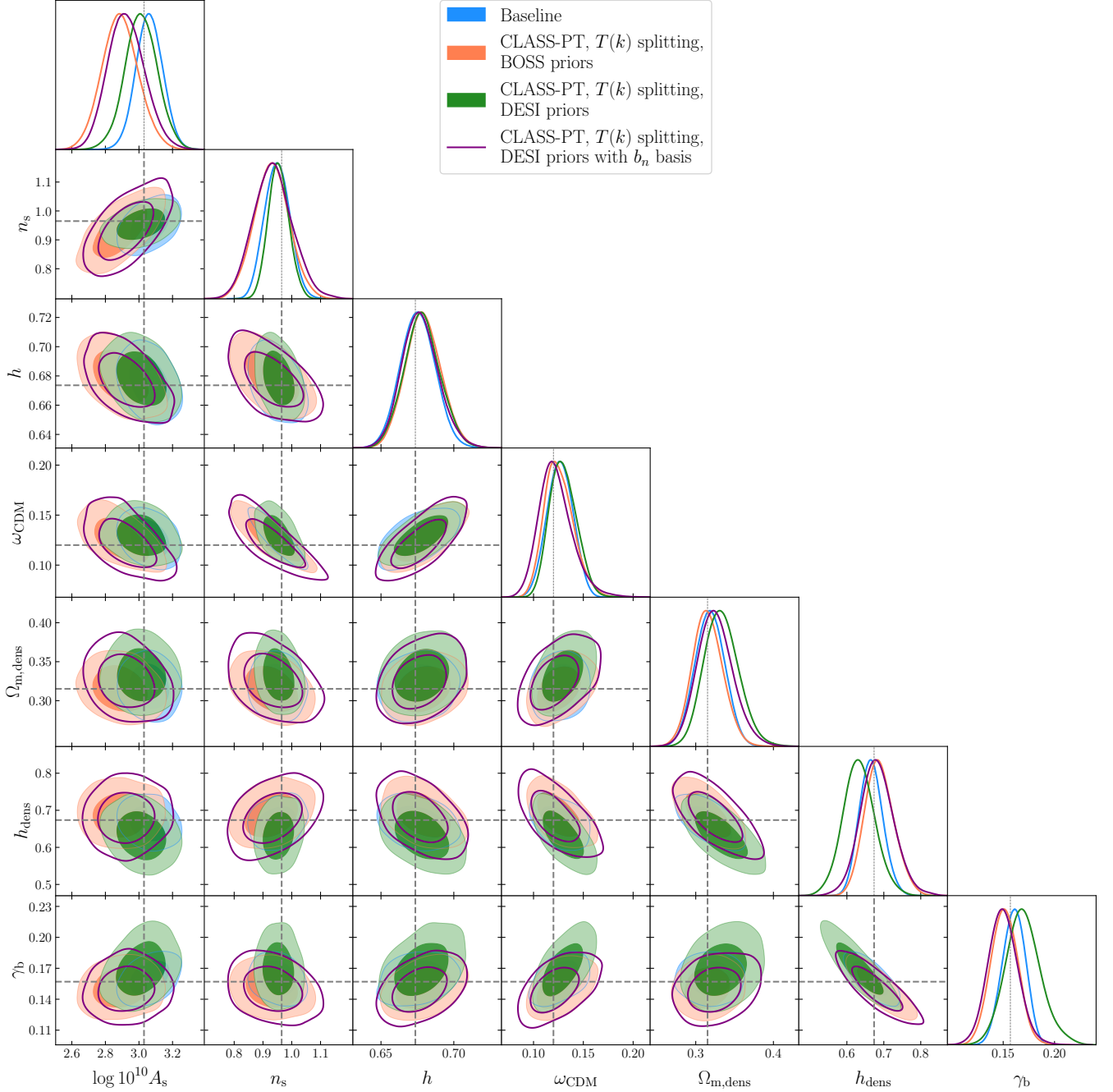


FIG. 10. Comparison of our results on Abacus mocks using different splitting methods and bias bases. The blue contours show the baseline results presented in the main body of the paper: **Velocileptors** EPT bias parameters with the HOD-informed prior to mitigate projection effects, using the consistent splitting of [43]. The orange contours show our old CLASS-PT pipeline used in [41] applied to the DESI mocks. The green contours show this same pipeline, but using the DESI bias priors, leading to large prior volume effects on γ_b and h^{dens} . The purple contours show the CLASS-PT pipeline with the DESI bias priors, but without rescaling the n^{th} order biases by σ_8^n . This produces very similar constraints to the bias prior used in [41], but mitigates projection effects on noiseless mocks.

eter set and the choice of whether to rescale the damping $C(k, \mu)$ by α (the baseline DESI analysis rescales $C(k, \mu)$ by α , whereas we rescale by α_{BB} instead).

Appendix D: Author affiliations

⁴Lawrence Berkeley National Laboratory, 1 Cyclotron Road, Berkeley, CA 94720, USA

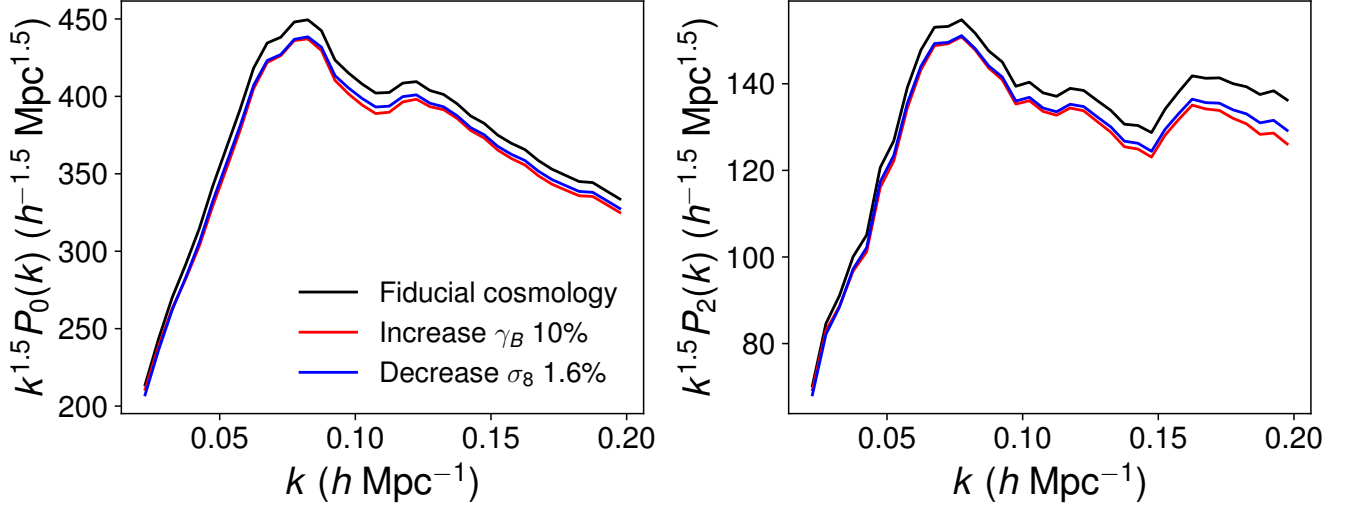


FIG. 11. Illustration of the γ_b - σ_8 degeneracy. Theory predictions for the monopole and quadrupole in the fiducial cosmology (black), a cosmology with 10% higher γ_b (red), and a cosmology with 1.6% lower σ_8 (blue). Due to the baryons' effect on the galaxy power spectrum shape, increasing γ_b suppresses the power spectrum on scales smaller than the baryonic Jeans scale. The degeneracy is broken by the more prominent BAO wiggles in models with larger γ_b .

Abacus run	Truth		h		γ_b	
	h	f_b	Mean $\pm 1\sigma$ (MAP)	$n\sigma$	Mean $\pm 1\sigma$ (MAP)	$n\sigma$
Baseline	0.6736	0.1571	0.665 ± 0.031 (0.662)	-0.28	0.160 ± 0.011 (0.160)	0.26
Baseline, HIP, $T(k)$ splitting	0.6736	0.1571	0.662 ± 0.030 (0.663)	-0.39	0.163 ± 0.011 (0.160)	0.54
Baseline, no HIP, $T(k)$ splitting	0.6736	0.1571	0.672 ± 0.031 (0.663)	-0.05	0.157 ± 0.011 (0.160)	-0.01
CLASS-PT, BOSS priors	0.6736	0.1571	$0.681^{+0.042}_{-0.037}$ (0.676)	0.21	$0.153^{+0.012}_{-0.013}$ (0.157)	-0.34
CLASS-PT, DESI priors b_n basis	0.6736	0.1571	$0.680^{+0.047}_{-0.043}$ (0.689)	0.16	$0.150^{+0.015}_{-0.014}$ (0.150)	-0.52
Λ CDM noiseless mocks						
Baseline	0.6736	0.1571	0.681 ± 0.037 (0.677)	0.20	0.155 ± 0.0144 (0.155)	-0.14
CLASS-PT, BOSS priors	0.6736	0.1571	$0.700^{+0.042}_{-0.040}$ (0.674)	0.66	$0.146^{+0.013}_{-0.012}$ (0.157)	-0.85
CLASS-PT, DESI priors b_n basis	0.6736	0.1571	0.681 ± 0.037 (0.674)	0.20	0.155 ± 0.014 (0.157)	-0.14
EDE noiseless mocks						
Baseline	0.7219	0.1471	0.721 ± 0.040 (0.716)	-0.03	0.1479 ± 0.015 (0.150)	0.05
DESI priors b_n basis	0.7219	0.1471	$0.706^{+0.046}_{-0.042}$	0.35	$0.144^{+0.013}_{-0.013}$	-0.21

TABLE VI. Summary of full-shape fits to the mean of the 25 Abacus mocks and noiseless theory vectors in both the default Λ CDM and early dark energy cosmologies. For the Abacus mocks, we compare results from different fitting pipelines, changing from the baseline analysis of this paper to the pipeline used in [41]. The top row shows the baseline approach, using **Effort.jl**, the consistent **CAMB** approach of [43] to model γ_b and the HOD-informed prior (HIP) to minimize prior volume effects. The next row shows the baseline approach, but instead using the old transfer function ($T(k)$) splitting from the BOSS analysis. The third row also omits the HOD-informed prior. The fourth and fifth rows in the Abacus runs compare the CLASS-PT pipeline, both with the priors used in the BOSS analysis and the priors matched to DESI (but constraining the bias parameters b_n rather than the combination $b_n\sigma_8^n$). The bottom rows show results on noiseless mocks, demonstrating that the BOSS priors used with CLASS-PT give large projection effects and therefore justifying our choice of the DESI priors with the b_n basis for the CLASS-PT pipeline.

Data combination	H_0^{dens} (km s $^{-1}$ Mpc $^{-1}$)	$\Omega_{\text{m,dens}}$	γ_b
Baseline (DESI DR1 galaxy clustering)	68.4 ± 3.6	0.301 ± 0.020	0.161 ± 0.010
Baseline, HIP, $T(k)$ splitting	68.1 ± 3.4	0.302 ± 0.019	0.162 ± 0.012
Baseline, no HIP, $T(k)$ splitting	69.9 ± 3.5	0.296 ± 0.020	0.157 ± 0.011
Baseline (DESI DR1 galaxy clustering + Ly α)	68.6 ± 3.1	0.301 ± 0.014	0.161 ± 0.010
CLASS-PT, DESI priors b_n basis (DESI DR1 galaxy clustering + Ly α)	$69.7^{+4.1}_{-3.7}$	$0.302^{+0.014}_{-0.013}$	0.153 ± 0.014

TABLE VII. Summary of full-shape fits to the DESI data for the baseline results (top) and different analysis choices, either using the CLASS-PT pipeline, or using the **Effort.jl** pipeline but with the transfer function split or no HOD-informed prior. The tests of the baseline pipeline were done using DESI DR1 galaxy clustering only, while the CLASS-PT pipeline run also includes Ly α BAO, so we compare it to the baseline pipeline run with Ly α BAO for consistency.

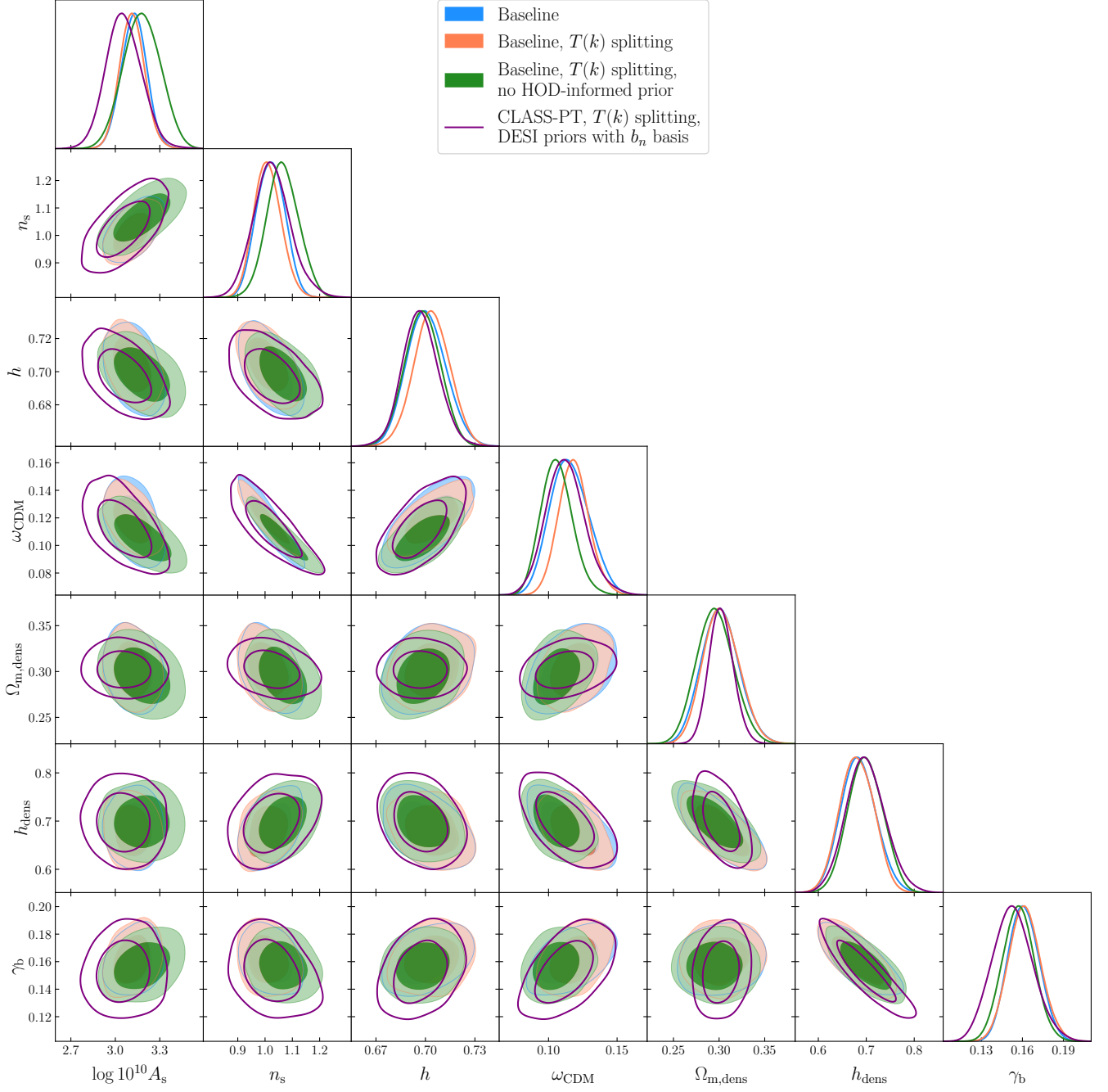


FIG. 12. Comparison of energy-density fits to DESI data using different fitting pipelines. The blue contours are the baseline full-shape fit results, using `Effort.jl`, the new approach of [43] for γ_b , and the HOD-informed prior. The orange and green contours show the same pipeline, but using the old transfer function based splitting (orange) or using the transfer function splitting and no HOD informed prior (green). The purple contours show the CLASS-PT pipeline used in [41], using the modified DESI prior basis.

Parameter	Default, γ_b	γ_b , $50 < r < 150 h^{-1} \text{ Mpc}$	DESI
BGS, $0.1 < z < 0.4$			
α_{iso}	0.9990 ± 0.0226	0.9967 ± 0.0194	0.994 ± 0.020
LRG, $0.4 < z < 0.6$			
α_{iso}	1.0061 ± 0.0155	1.0043 ± 0.0154	0.9978 ± 0.0135
α_{AP}	1.0084 ± 0.0547	1.0087 ± 0.0642	0.9897 ± 0.0478
LRG, $0.6 < z < 0.8$			
α_{iso}	0.9995 ± 0.0111	0.9991 ± 0.0114	0.9946 ± 0.0111
α_{AP}	1.0106 ± 0.0392	1.0145 ± 0.0403	1.0081 ± 0.036
LRG+ELG, $0.8 < z < 1.1$			
α_{iso}	1.0038 ± 0.0085	1.0015 ± 0.0085	0.9990 ± 0.0084
α_{AP}	0.9960 ± 0.0277	1.0011 ± 0.0290	0.9930 ± 0.0352
ELG, $1.1 < z < 1.6$			
α_{iso}	1.0032 ± 0.0160	0.9980 ± 0.0157	0.9949 ± 0.015
α_{AP}	1.0037 ± 0.0555	1.0104 ± 0.0575	0.9986 ± 0.051
QSO, $0.8 < z < 2.1$			
α_{iso}	0.9928 ± 0.0179	0.9991 ± 0.0172	0.995 ± 0.018

TABLE VIII. Comparison of BAO scaling parameters (the median of the 25 Abacus altmtml mocks, and the median of their errors) in our pipeline with its default settings (left); our pipeline matching the DESI fitting range $50 < r < 150 h^{-1} \text{ Mpc}$ (center); and the default DESI pipeline from Table 9 in [61]. Unlike in Table II, all α parameters are relative to the DESI fiducial cosmology.

Pipeline	α_{iso}	$\sigma_{\alpha_{\text{iso}}}$	α_{AP}	$\sigma_{\alpha_{\text{AP}}}$
DESI	0.998	0.014	0.990	0.048
BAO Amp.	1.006	0.016	1.008	0.055
Match fitting range	1.004	0.015	1.009	0.064
DESI priors on $\Sigma_{\parallel, \perp, \text{fog}}$, $\alpha_{\text{BB}} = 1$, fix γ_b , $b_{\partial} = 0$	1.003	0.014	1.004	0.051
Sample in $\alpha_{\text{iso}, \text{AP}}$	1.000	0.014	1.001	0.050
Parameterize bias with b_1 and f	0.999	0.014	1.004	0.048
Rescale $C(k, \mu)$ by α	0.999	0.014	0.999	0.048

TABLE IX. Detailed comparison of our results and the default DESI results for LRG $0.4 < z < 0.6$. The first three rows reproduce the three columns of Table VIII.

⁵Department of Physics, Boston University, 590 Commonwealth Avenue, Boston, MA 02215 USA

⁶Dipartimento di Fisica “Aldo Pontremoli”, Università degli Studi di Milano, Via Celoria 16, I-20133 Milano, Italy

⁷INAF-Osservatorio Astronomico di Brera, Via Brera 28, 20122 Milano, Italy

⁸Department of Physics & Astronomy, University College London, Gower Street, London, WC1E 6BT, UK

⁹Institute of Cosmology and Gravitation, University of Portsmouth, Dennis Sciamia Building, Portsmouth, PO1 3FX, UK

¹⁰Institute for Computational Cosmology, Department of Physics, Durham University, South Road, Durham DH1 3LE, UK

¹¹Instituto de Física, Universidad Nacional Autónoma de México, Circuito de la Investigación Científica, Ciudad Universitaria, Cd. de México C. P. 04510, México

¹²Department of Astronomy, San Diego State University, 5500 Campanile Drive, San Diego, CA 92182, USA

¹³NSF NOIRLab, 950 N. Cherry Ave., Tucson, AZ 85719, USA

¹⁴Space Sciences Laboratory, University of California, Berkeley, 7 Gauss Way, Berkeley, CA 94720, USA

¹⁵University of California, Berkeley, 110 Sproul Hall #5800 Berkeley, CA 94720, USA

¹⁶Institut de Física d’Altes Energies (IFAE), The Barcelona Institute of Science and Technology, Edifici Cn, Campus UAB, 08193, Bellaterra (Barcelona), Spain

¹⁷Departamento de Física, Universidad de los Andes, Cra. 1 No. 18A-10, Edificio Ip, CP 111711, Bogotá, Colombia

¹⁸Observatorio Astronómico, Universidad de los Andes, Cra. 1 No. 18A-10, Edificio H, CP 111711 Bogotá, Colombia

¹⁹Institut d’Estudis Espacials de Catalunya (IEEC), c/ Esteve Terradas 1, Edifici RDIT, Campus PMT-UPC, 08860 Castelldefels, Spain

²⁰Institute of Space Sciences, ICE-CSIC, Campus UAB, Carrer de Can Magrans s/n, 08913 Bellaterra, Barcelona, Spain

²¹University of Virginia, Department of Astronomy, Charlottesville, VA 22904, USA

²²Fermi National Accelerator Laboratory, PO Box 500, Batavia, IL 60510, USA

²³Institut d’Astrophysique de Paris. 98 bis boulevard Arago. 75014 Paris, France

²⁴IRFU, CEA, Université Paris-Saclay, F-91191 Gif-sur-Yvette, France

²⁵Center for Cosmology and AstroParticle Physics, The Ohio State University, 191 West Woodruff Avenue, Columbus, OH 43210, USA

²⁶Department of Physics, The Ohio State University, 191 West Woodruff Avenue, Columbus, OH 43210, USA

²⁷The Ohio State University, Columbus, 43210 OH, USA

²⁸Department of Physics, University of Michigan, 450 Church Street, Ann Arbor, MI 48109, USA

²⁹University of Michigan, 500 S. State Street, Ann

Arbor, MI 48109, USA

³⁰Department of Physics, The University of Texas at Dallas, 800 W. Campbell Rd., Richardson, TX 75080, USA

³¹Department of Physics, Southern Methodist University, 3215 Daniel Avenue, Dallas, TX 75275, USA

³²Department of Physics and Astronomy, University of California, Irvine, 92697, USA

³³Sorbonne Université, CNRS/IN2P3, Laboratoire de Physique Nucléaire et de Hautes Energies (LPNHE), FR-75005 Paris, France

³⁴Departament de Física, Serra Húnter, Universitat Autònoma de Barcelona, 08193 Bellaterra (Barcelona), Spain

³⁵Institució Catalana de Recerca i Estudis Avançats, Passeig de Lluís Companys, 23, 08010 Barcelona, Spain

³⁶Department of Physics and Astronomy, Siena University, 515 Loudon Road, Loudonville, NY 12211, USA

³⁷Departamento de Física, DCI-Campus León, Universidad de Guanajuato, Loma del Bosque 103, León, Guanajuato C. P. 37150, México

³⁸Instituto Avanzado de Cosmología A. C., San Marcos

11 - Atenas 202. Magdalena Contreras. Ciudad de México C. P. 10720, México

³⁹Instituto de Astrofísica de Andalucía (CSIC), Glorieta de la Astronomía, s/n, E-18008 Granada, Spain

⁴⁰Departament de Física, EEBE, Universitat Politècnica de Catalunya, c/Eduard Maristany 10, 08930 Barcelona, Spain

⁴¹Department of Physics and Astronomy, Sejong University, 209 Neungdong-ro, Gwangjin-gu, Seoul 05006, Republic of Korea

⁴²Abastumani Astrophysical Observatory, Tbilisi, GE-0179, Georgia

⁴³Department of Physics, Kansas State University, 116 Cardwell Hall, Manhattan, KS 66506, USA

⁴⁴Faculty of Natural Sciences and Medicine, Ilia State University, 0194 Tbilisi, Georgia

⁴⁵CIEMAT, Avenida Complutense 40, E-28040 Madrid, Spain

⁴⁶National Astronomical Observatories, Chinese Academy of Sciences, A20 Datun Road, Chaoyang District, Beijing, 100101, P. R. China